AGU PUBLICATIONS

Tectonics

RESEARCH ARTICLE
10.1002/2015TC004007

Key Points:
- In the upper mantle strain localizes along mechanical anisotropies
- Continuous shear zone narrowing with progressive cooling
- Transition from melt-assisted to solid-state to fluid-assisted deformation

Correspondence to:
M. Herwegh,
marco.herwegh@geo.unibe.ch

Citation:
Herwegh, M., I. Mercolli, J. Linckens, and O. Müntener (2016), Mechanical anisotropy control- on strain localization in upper mantle shear zones, *Tectonics*, *35*, 1177–1204, doi:10.1002/2015TC004007.

Received 14 AUG 2015
Accepted 22 APR 2016
Accepted article online 27 APR 2016
Published online 20 MAY 2016

Mechanical anisotropy control on strain localization in upper mantle shear zones

Marco Herwegh[1], Ivan Mercolli[1], Jolien Linckens[1,2], and Othmar Müntener[3]

[1]Institute of Geological Sciences, University of Bern, Bern, Switzerland, [2]Now at Institut für Geowissenschaften, Goethe University of Frankfurt, Frankfurt, Germany, [3]Institute of Earth Sciences, University of Lausanne, Lausanne, Switzerland

Abstract Mantle rocks at oceanic spreading centers reveal dramatic rheological changes from partially molten to solid-state ductile to brittle deformation with progressive cooling. Using the crustal-scale Wadi al Wasit mantle shear zone (SZ, Semail ophiolite, Oman), we monitor such changes based on quantitative field and microstructural investigations combined with petrological and geochemical analyses. The spatial distribution of magmatic dikes and high strain zones gives important information on the location of magmatic and tectonic activity. In the SZ, dikes derived from primitive melts (websterites) are distributed over the entire SZ but are more abundant in the center; dikes from more evolved, plagioclase saturated melts (gabbronorites) are restricted to the SZ center. Accordingly, harzburgite deformation fabrics show a transition from protomylonite (1100°C), mylonite (900–800°C) to ultramylonite (<700°C) and a serpentine foliation (<500°C) from the SZ rim to the center. The spatial correlation between solid-state deformation fabrics and magmatic features indicates progressive strain localization in the SZ on the cooling path. Three stages can be discriminated: (i) Cycles of melt injection (dunite channels and websterite dikes) and solid-state deformation (protomylonites-mylonites; 1100–900°C), (ii) dominant solid-state deformation in harzburgite mylonites (900–800°C) with some last melt injections (gabbronorites) and ultramylonites (<700°C), and (iii) infiltration of seawater inducing a serpentine foliation (<500°C) followed by cataclasis during obduction. The change of these processes in space and time indicates that early dike-related ridge-parallel deformation controls the onset of the entire strain localization history promoting nucleation sites for different strain weakening processes as a consequence of changing physicochemical conditions.

1. Introduction

Mid-ocean ridges are important plate boundaries, where new crust is formed and intense seismic and magmatic activity is documented. While the access to active ridges often is difficult, exhumed paleo-mid-ocean ridges provide the unique opportunity to gain insights into the associated 3-D deformation pattern and its temporal and spatial evolution during spreading. Particularly because of the initial high-temperature conditions at the ridge and the subsequent fast cooling with progressive spreading, the entire succession and interplay from early melt-assisted to high-temperature solid-state to low-temperature alteration under the presence of seawater can be studied at such sites.

Formation of oceanic crust at mid-ocean ridges by crystallization of magmas formed by decompression of the asthenosphere [*Kawakatsu et al*., 2009; *Schmerr*, 2012] is one of the fundamental processes on Earth. During magma ascent, deformation of the associated host rocks plays a fundamental role. Mechanical models suggested that dike injection represents the major pathways for magma emplacement at shallow crustal levels [*Buck et al*., 2005; *Behn and Ito*, 2008; *Ito and Behn*, 2008], while in the mantle focused porous flow may be the dominant transport mechanism [*Kelemen et al*., 1995]. Based on growing knowledge from deep-sea drilling and submersible surveys, axial faulting might provide additional conduits for rising magmas [e.g., *Hayman and Karson*, 2009]. In the latter model, magma follows brittle high strain zones, which are cyclically overprinted in a complex manner by brittle fracturing/cataclasis, infiltration of seawater, chemical alteration, and cementation of the fault rocks. Little is known, however, about the structure and mechanical behavior of such fault zones, their continuation with depth, and if and how melt migrates along such structures. The occurrence of subvertical fossil high strain zones of exhumed upper mantle rocks [e.g., *Boudier et al*., 1988; *Dijkstra et al*., 2002; *Newman et al*., 1999; *Michibayashi and Mainprice*, 2004; *Toy et al*., 2010; *Linckens et al*., 2015] as well as seismic activity [e.g. *Dziak et al*., 1995; *Passarelli et al*., 2014] suggests localized deformation in the lithospheric mantle. Particularly, seismic activity in the vicinity of ridge axes points toward cycles of fast brittle and slow ductile deformation.

In terms of melt generation and melt extraction in the asthenosphere, grain-scale porous flow is considered to represent the fundamental process [*Aharonov et al*., 1995, 1997; *Kelemen et al*., 1997b; *Ceuleneer et al*., 1996; *Spiegelman et al*., 2001; *Dijkstra et al*., 2002; *Weatherley and Katz*, 2012]. For the subsequent melt ascent, the following three major flow types have been suggested: (i) diapirism [e.g., *Ceuleneer et al*., 1988; *Nicolas et al*., 1988], (ii) compaction channeling [e.g., *Scott*, 1988] in porosity waves [*Connolly and Podladchikov*, 1998], and (iii) tensile fracturing (diking) [e.g., *Ito and Martel*, 2002; *Choi et al*., 2008; *Choi and Buck*, 2010; *Havlin et al*., 2013]. Recent numerical modeling by *Keller et al.* [2013] indicates that the dominant process (i), (ii), or (iii) strongly depends on the viscosities of the host rocks, which are low, intermediate, or high, respectively. For (i), melt rises buoyantly in pulses rather than in a continuous flow. For (ii) overpressurized melt pockets induce localized melt pathways by intergranular fracturing on the millimeter to centimeter scale, where compaction waves in combination with shear stresses and buoyancy force melt ascent. In the case of (iii), host rock failure occurs via hydrofracturing during shearing. In the current study we follow two major goals: (a) We first evaluate how melt migration and deformation interact during the early high-temperature part of shearing. It will become evident that mechanical anisotropies, evolved after the onset of magmatic activity and the crystallization of early pyroxenites, force the successive magmatic and deformational activity to juxtapose in a complex three-dimensional manner. Our field evidence indicates synchronous strain localization and magma emplacement associated with differentiation of magma during early stages of strain localization. (b) With progressive spreading and shearing, the system cools and we unravel the effect of the initially formed mechanical anisotropies on the retrograde strain localization under solid-state conditions including the alteration by seawater once the system embrittles. We address these aspects by investigating in detail the exhumed Wadi al Wasit shear zone located in the mantle section of the Semail ophiolite (Oman, Figure 1).

2. Geological Setting

2.1. Temporal Framework of the Evolution of the Semail Ophiolite

The mantle section of the Semail ophiolite (Oman) is one of the largest and best exposed worldwide allowing the study of upper mantle deformation near the crust-mantle boundary (Figure 1) [*Nicolas et al*., 1994a,1994b; *Boudier and Nicolas*, 1985; *Michibayashi et al*., 2000; *Dijkstra et al*., 2002]. Mantle diapirs, as mapped by changes from vertical to horizontal flow lines in harzburgites, overlain by gabbros, sheeted dikes, and basaltic lavas, provoked the notion of mantle upwelling and continuous spreading (Figure 1) [*Ceuleneer et al*., 1988; *Nicolas et al*., 1988, 1989, 1994a; *Gnos and Nicolas*, 1996; *Hacker and Gnos*, 1997; *Searle and Cox*, 1999]. The geodynamic context is still a matter of debate. However, it is generally accepted that the magmatic activity in the Semail ophiolite can be split into two stages:

1. The first magmatic event is mainly recorded in the central and southern areas of the Semail ophiolite, shows mid-ocean ridge basalt (MORB) signatures, and forms a Penrose type [*Anonymous*, 1972] oceanic crustal sequence. U-Pb dating on zircons indicates that the main phase was active between ~96.25 and 95.5 Ma (e.g., see *Warren et al*. [2005], *Rioux et al*. [2012], and *Rioux et al*. [2013] for discussion on error bars). Given the volume of mafic magmas and the similarity with the seismically defined structure of fast spreading ridges, the Semail ophiolite was considered to be a fossil example of a fast-spreading ridge [*Boudier and Coleman*, 1981; *Reid and Jackson*, 1981; *Boudier and Nicolas*, 1985; *Boudier et al*., 1988; *Nicolas*, 1989; *Gnos and Nicolas*, 1996; *Nicolas et al*., 2000; *Ishikawa et al*., 2002; *Godard et al*., 2003; *Ishikawa et al*., 2005; *Godard et al*., 2006; *Rioux et al*., 2013]. For these reasons, a transform fault/mid-ocean ridge model was suggested, where obduction along the basal thrust was southward directed, close to the ridge, resulting in ridge-parallel strike-slip shear zones [*Boudier et al*., 1988; *Hacker et al*., 1996]. In an advanced stage, the southward movement changed to west directed obduction onto the Arabian shield.
2. The second magmatic stage, mainly expressed in the northern blocks of the ophiolite, is only slightly younger than the first one (~95.4–95.0 Ma, *Rioux et al.* [2013]; *Warren et al.* [2005]). It shows geochemical signatures characteristic for subduction-related magmatism delivering the argument for a suprasubduction zone origin of the ophiolite [*Searle et al*., 1980; *Searle and Malpas*, 1980; *Pearce et al*., 1981; *Searle and Malpas*, 1982; *Searle and Cox*, 1999, 2002; *Warren et al*., 2005; *MacLeod et al*., 2013]. Accordingly, subduction initiation along a former strike-slip fault was proposed, followed by roll-back of the subducting plate. The roll-back leads to fast spreading and ridge formation in the upper plate followed by obduction along the subduction zone thrust [*Lippard et al*., 1986; *Gnos and Nicolas*, 1996; *Searle and Cox*, 1999]. The

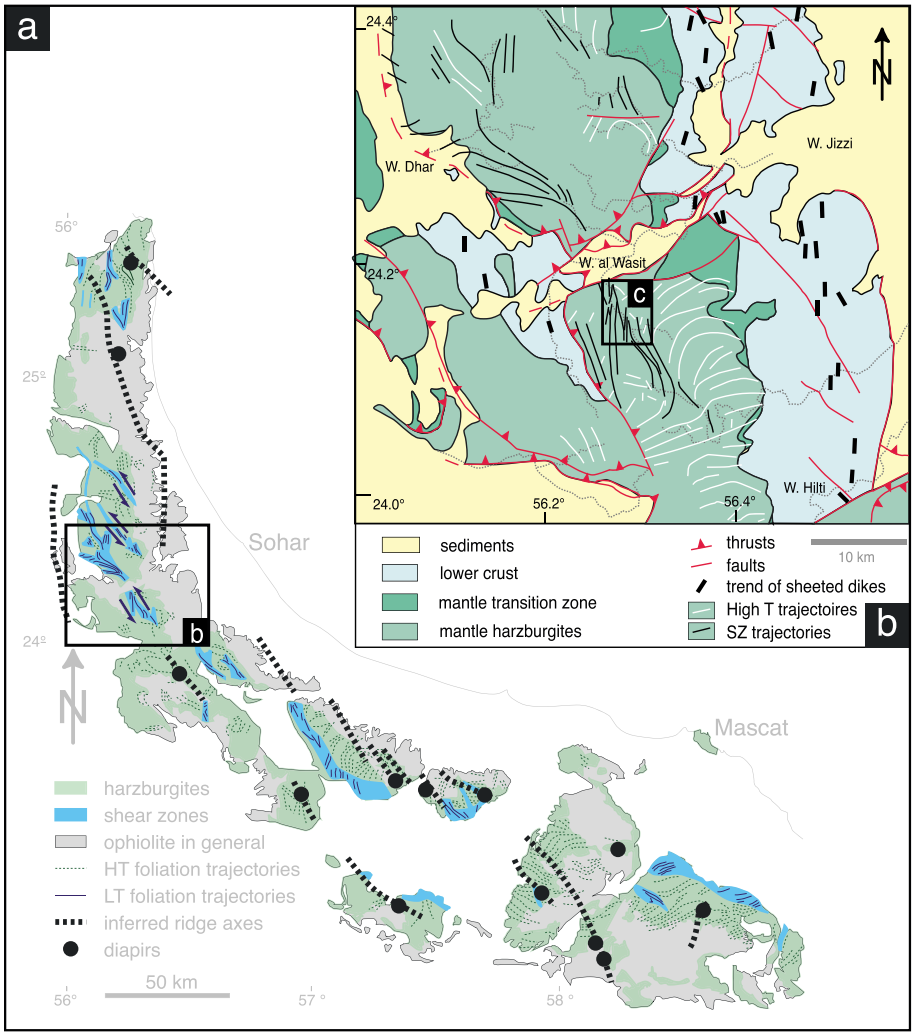

Figure 1. (a) Map of shear zones, mantle diapirs, and inferred ridge axes (compiled after structural map of the Semail ophiolite [*Nicolas et al.*, 2000; *Python and Ceuleneer*, 2003]). (b) Geologic overview of the (c) field area located in the Hilti massif of the Semail ophiolite (b: modified after *Nicolas et al.* [2000] and *Michibayashi and Mainprice* [2004]). Note the N-S trending sheeted dikes in the lower-middle crust as indicators of the orientation of the paleoridge orientation and the NNW-SSE striking shear zones (SZ) in the mantle harzburgites.

suprasubduction zone model is currently favored by different authors [*Rioux et al.*, 2013 and references therein]. Given the U-Pb dates of these authors, the time interval between formation of oceanic crust in the first magmatic event and subsequent injection of younger dikes during the second magmatic event must be < 0.25–0.5 Ma.

Because of similarities with the Izu-Bonin-Mariana forearc, recently, forearc or incipient subduction models were suggested as an alternative to the suprasubduction zone models, the later related to a back-arc basin extensional environment [*Whattam and Stern*, 2011; *Ishikawa et al.*, 2002; *Ishizuka et al.*, 2014].

2.2. Dikes in the Mantle Sequence

Numerous dikes cross cut the mantle sequence and are correlated with the two aforementioned magmatic suites [*Nicolas et al.*, 2000; *Python and Ceuleneer*, 2003]. (i) Troctolite and olivine gabbro dikes intruded at about 1200°C and derived from fractional crystallization of primitive MORB melts [*Nicolas et al.*, 1994b; *Kelemen et al.*, 1997a; *Koga et al.*, 2001]. They are exposed almost exclusively in elongated zones with orientation parallel to the sheeted dikes of the midcrust and lower crust, suggesting formation during

asthenospheric upwelling and spreading [*Nicolas et al*., 1994b; *Python and Ceuleneer*, 2003]. (ii) In contrast, pyroxenite (websterite), gabbronorite, diorite, and trondhjemite dikes formed from a more depleted mantle source after melt extraction of (i). Based on the lack of chilled margins and the frequent coarse-grained to pegmatitic texture of the latter dikes, *Python and Ceuleneer* [2003] suggested that they intruded into colder harzburgites (600–1100°C). They are therefore younger and unrelated to (i). These dikes formed from melts enriched in SiO_2 but depleted in incompatible elements (Na, Ti) and light REE (LREE) [*Kelemen et al*., 1997a; *Boudier et al*., 2000; *Python and Ceuleneer*, 2003]. *Rioux et al.* [2012, 2013] describe negative ε_{Nd} for two trondhjemites intruding the mantle harzburgite suggesting a mixing with a new melt source, derived from older oceanic crust and/or metamorphosed sediments in a suprasubduction scenario.

In agreement with the observed difference of spatial distribution of the two magmatic suites, troctolites and olivine gabbros mainly occur in the vicinity of the diapirs in the SE and few in the NW of the Semail ophiolite, while pyroxenites (websterites) and gabbronorites are found in the remaining parts of the mantle sequence [see *Python and Ceuleneer*, 2003, their Figure 19]. Despite the general trend of mafic dikes to be oriented subparallel to the basaltic dikes of the sheeted dike complex [*Nicolas et al*., 2000], the study of *Python and Ceuleneer* [2003] reveals dike-specific variations in their orientation. Troctolites show variable orientations in strike and dip but the olivine gabbros are subvertical and parallel to the sheeted dikes. The depleted dike suite shows more complex orientations, sometimes being parallel in strike and dip to the sheeted dikes, sometimes showing nearly random orientations [see *Python and Ceuleneer*, 2003, their Figure 20].

2.3. Solid-State Deformation

Deformation in the mantle sequence of the Semail ophiolite is initially accompanied by magmatic activity during ridge-related asthenospheric flow and progressive development of solid-state deformation during retrograde cooling [*Boudier et al*., 1988]. Ridge-related asthenospheric flow at high-medium temperatures (HT 1100°C) resulted in a transition from equigranular to porphyroclastic fabrics [*Boudier et al*., 1985; *Nicolas*, 1986; *Boudier et al*., 1988; *Ceuleneer et al*., 1988; *Dijkstra et al*., 2002; *Linckens et al*., 2011a, 2011b; *Linckens et al*., 2015]. These fabrics are overprinted by low-temperature (900–800°C) ductile deformation of the peridotite as documented by transitions from the porphyroclastic fabrics via protomylonites to mylonites [*Boudier et al*., 1985; *Nicolas*, 1986; *Boudier et al*., 1988; *Dijkstra et al*., 2002; *Michibayashi and Mainprice*, 2004; *Michibayashi et al*., 2006; *Linckens et al*., 2011a, 2011b, 2015]. Ultramylonites reveal a final stage of ductile shearing (700–800°C), which is restricted to polymineralic bands in the harzburgite [*Linckens et al*., 2011a, 2011b].

2.4. Solid-State Deformation in the Wadi al Wasit Shear Zone

The Wadi al Wasit shear zone is located at the western end of the Hilti Massif (Semail ophiolite, Oman, Figure 1). This mantle section and the overlaying crustal sequence are tilted by 25° toward the east [*Ildefonse et al*., 1995] exposing deeper mantle sections in the west, where the shear zone is situated (Figure 1). Here the exposed harzburgitic upper mantle is located 2–5.5 km below the former crust-mantle boundary [*Michibayashi et al*., 2000; *Dijkstra et al*., 2002]. The large-scale shear zone belongs to a set of vertical N-S and NW-SE trending strike-slip faults with dextral and sinistral senses of shear, respectively [*Boudier et al*., 1988; *Michibayashi and Mainprice*, 2004; *Michibayashi et al*., 2006]. The shear zone exposes a variety of fabrics suggesting transitions from magmatic to solid-state flow (see below).

In the study area, porphyroclastic microfabrics represent a small volume fraction only (Figure 1). They are characterized (Figures 4a and 4d) by coarse-grained enstatite and diopside prophyroclasts (2–6 mm) embedded in finer-grained polymineralic domains consisting of orthopyroxene (~100 μm), olivine (~300 μm), spinel (~60 μm), and clinopyroxene (~150 μm). The bulk rheology of the harzburgite at about 1100°C is controlled by olivine [*Linckens et al*., 2011a]. Its strong crystallographic preferred orientation (CPO) suggests dislocation creep as the dominant deformation mechanism [see *Linckens et al.*, 2011b, their Figure 6].

Continuous deformation during retrograde cooling induced strain localization and the formation of mylonites at 900–800°C (Figures 4b, 4c, and 4e), in the N-S trending shear zones [*Boudier et al*., 1988; *Michibayashi and Mainprice*, 2004; *Michibayashi et al*., 2006; *Linckens et al*., 2011a] (Figure 2). The original foliation of asthenospheric ridge-related flow was N-S trending but shows variable dip angles as can be recognized from remnants not affected by solid-state shearing (Figures 2 and 3a). Sinistral strike-slip

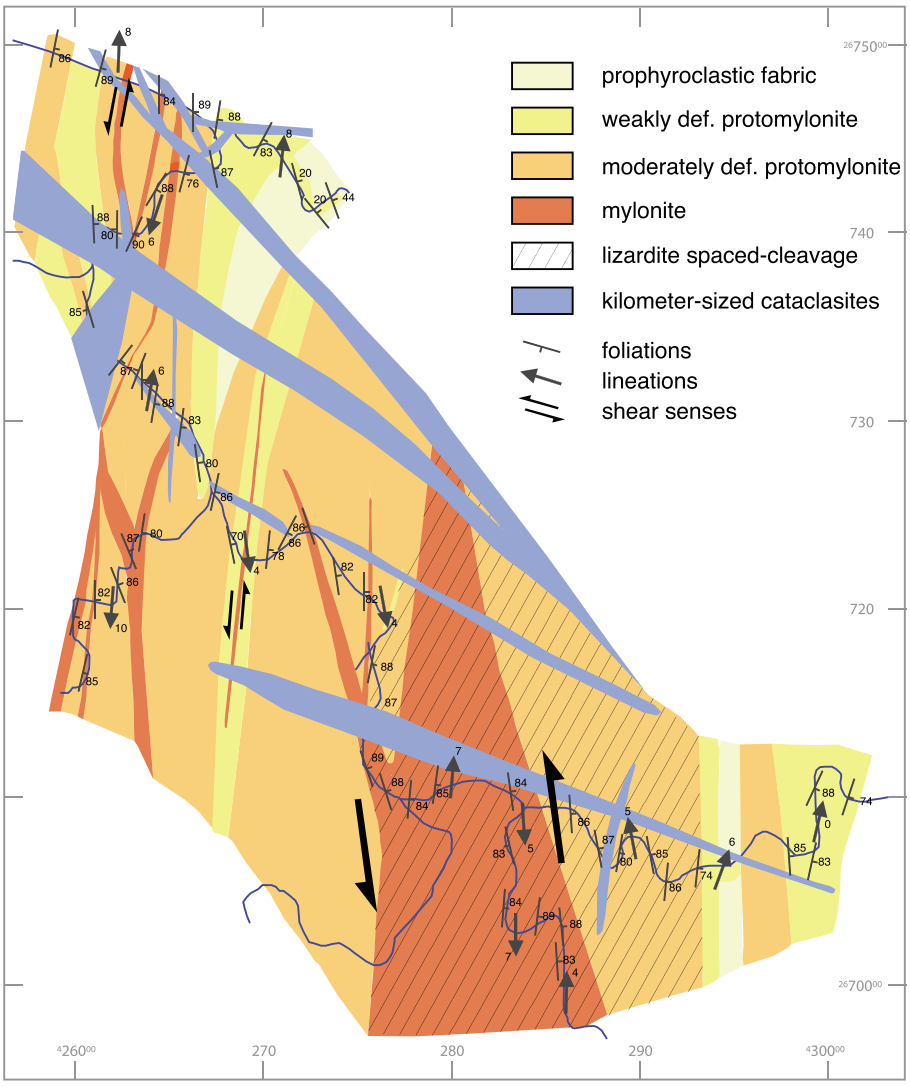

Figure 2. Geological map showing the spatial distribution of the different tectonites of the large-scale mantle shear zone crossed by Wadi al Wasit (Hilti Massif, see Figure 1). Mylonites of the shear zone as well as associated foliations and lineations are preferentially N-S oriented. The shear zone center is overprinted by an NNE-SSW trending lizardite spaced-cleavage. All structures are dissected by late cataclastic overprint (blue). One kilometer geographic grid. Modified after *Linckens et al.* [2011a]. Location of figure shown as inset (c) in Figure 1.

deformation resulted in sub vertical foliations (Figures 3c and 3e) and horizontal lineations (Figures 3d and 3f) in a major 500 m wide sinistral mylonitic shear zone (Figure 2). In addition, several centimeter-wide mylonitic shear zones formed either parallel to the major structures or as slightly oblique connections between them (Figure 2). In the large-scale shear zone the evolved strain gradients are macroscopically detectable and mappable by increasingly elongated orthopyroxene (opx) resulting in gradual transitions from weakly deformed protomylonites to moderately deformed protomylonites and into mylonites from shear zone rim to core, respectively [*Linckens et al.*, 2011b, 2015]. Substantial grain size reduction from the protomylonites to the mylonites (800 μm to 300 μm) at the microscale is accommodated by subgrain rotation recrystallization in monomineralic olivine-rich domains (Figures 4e and 4f). In polymineralic domains with increasing strain, the grain sizes of olivine and all secondary phases (spinel, opx, and cpx) are reduced [*Linckens et al.*, 2011b, Figure 4] by a combination of neocrystallization and recrystallization, mass transfer processes, and grain boundary sliding [*Linckens et al.*, 2011b, 2015]. Here Zener pinning (pinning of the olivine grain boundaries by pyroxenes and spinel) controls the olivine grain size [*Linckens et al.*, 2011b; *Herwegh et al.*, 2011]. The

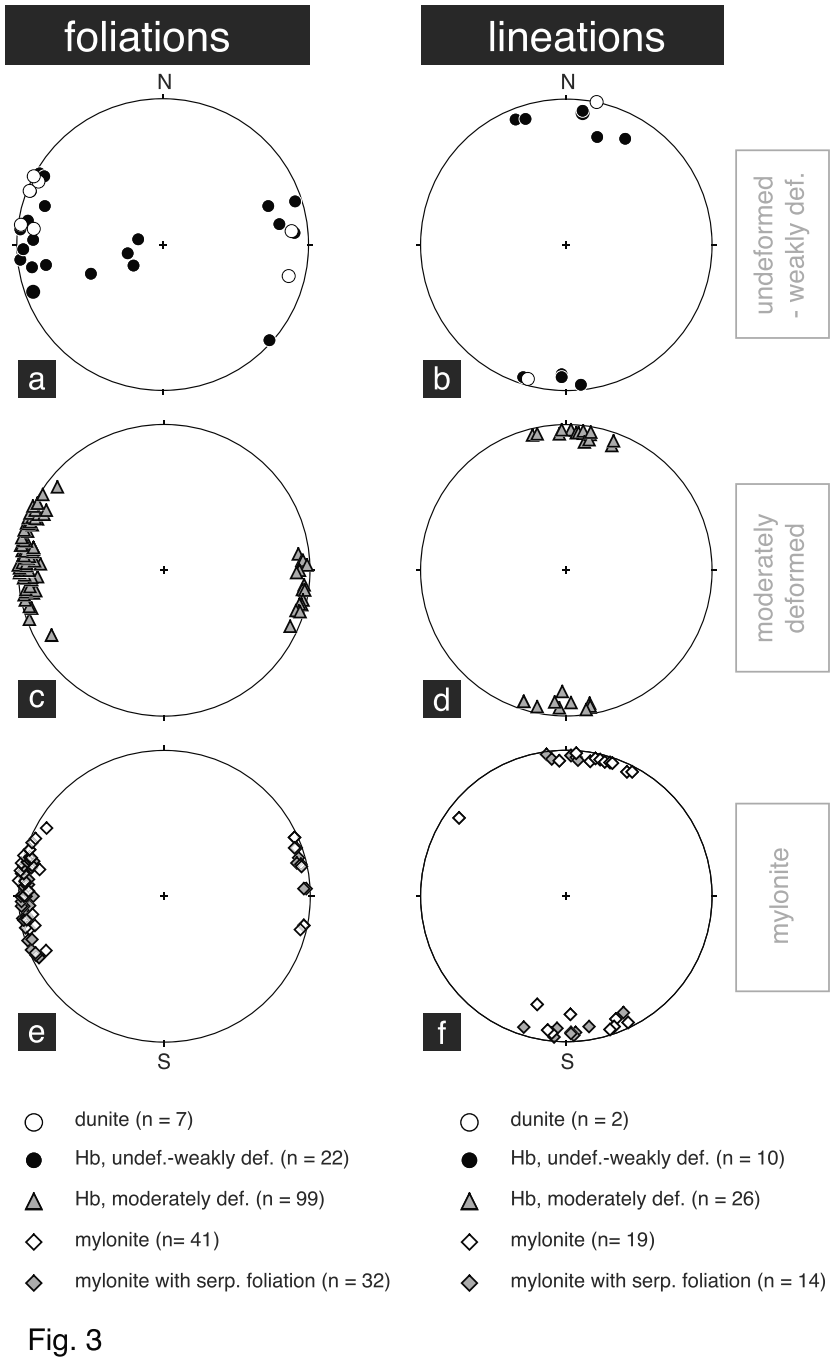

Fig. 3

Figure 3. Stereographic projections of N-S trending foliations and lineations with increasing shear strain (top-down) in the harzburgites (Hb). Foliations in the porphyroclastic fabrics to weakly deformed protomylonites are preferentially related to (a) early spreading-related flow. They vary in dip around a N-S oriented rotation axis, while all foliations of the (c) moderately deformed protomylonites and mylonites of the (e) solid-state shear zone are N-S trending and subvertical. (b, d, and f) All lineations are horizontal and N-S trending; *n*: number of data.

CPOs of both monomineralic and polymineralic mylonites are strong but somewhat weaker in the case of the latter [*Linckens et al.*, 2011b, their Figure 6]. The dominant deformation mechanisms during strain localization in the temperature range of 900–800°C were dislocation creep and dislocation accommodated grain boundary sliding in monomineralic olivine and polymineralic domains, respectively [*Linckens et al.*, 2011b, 2015].

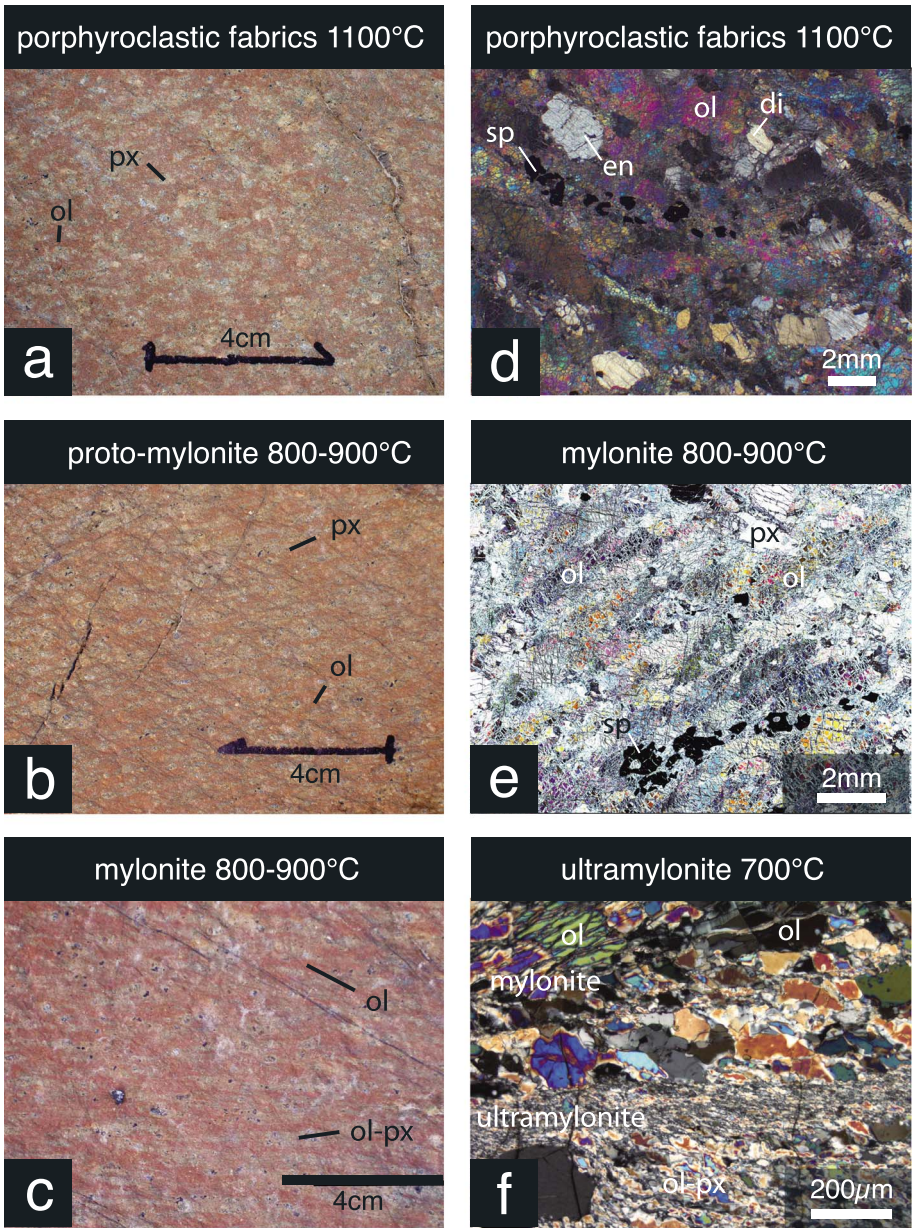

Figure 4. (a–c) Macroscopic and (d–f) microscopic appearance of harzburgite (px: pyroxenes, ol: olivine) at various deformation stages and (Figures 4e and 4f) corresponding microfabrics (ol: olivine; en: enstatite; di: diopside; and sp: spinel). Note that olivine represents an interconnected matrix from porphyroclastic to mylonitic microstructures. Only in the case of the ultramylonites olivine aggregates exist as isolated lenses embedded in an ultrafine-grained polymineralic matrix consisting of olivine, enstatite, and diopside as well as very minor amounts of spinel.

With progressive cooling, at temperatures around 700°C, strain is further localized resulting in very narrow ($<$300 μm) ultramylonitic bands (Figure 4f) in the central parts of the major shear zone [*Linckens et al.*, 2011b]. These bands are polymineralic and consist of equiaxed, ultrafine recrystallized grains (ol $<$ 60 μm; opx, cpx, spinel all $<$ 15 μm; Figure 4 in *Linckens et al.*, 2011b). The olivine CPO is rather weak [*Linckens et al.*, 2011b, Figure 6]. In addition, *Michibayashi and Mainprice* [2004] found lenses of coarser grained monomineralic olivine embedded within the ultramylonitic matrix. *Linckens et al.* [2011b, 2015] interpret these observations as concentration of deformation in the polymineralic ultramylonites under diffusion creep conditions, while the deformation temperatures were too cold to allow for efficient ductile deformation in monomineralic olivine aggregates.

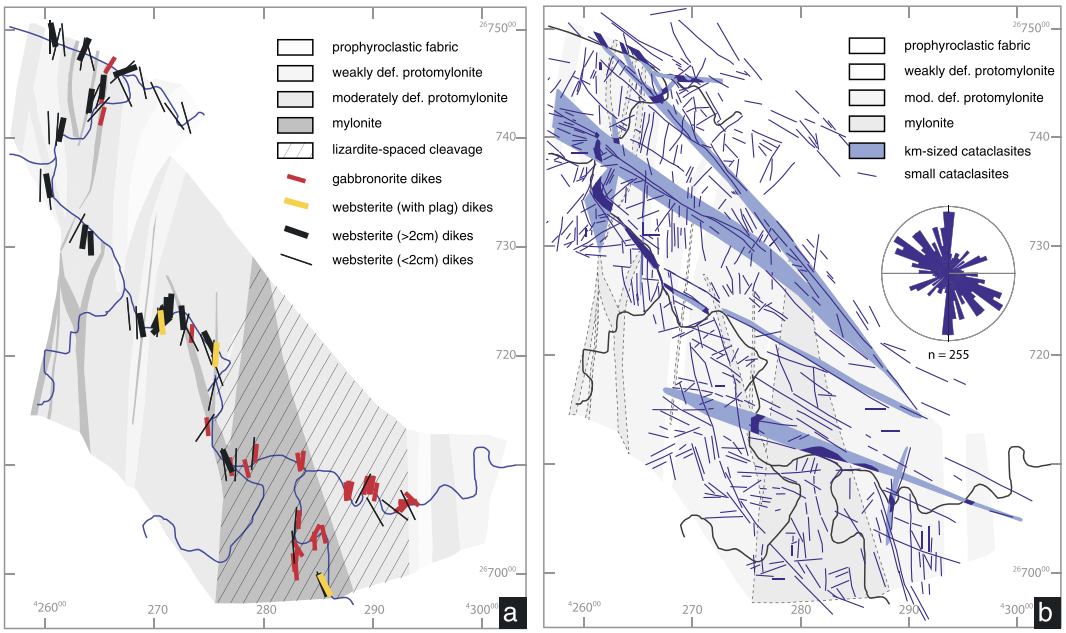

Figure 5. Map showing the spatial distribution of (a) the different dikes and (b) cataclasites. Map of the tectonites in grey shades (cf. Figure 2). (Figure 5a) All dikes show N-S trends. Note the correlation between the occurrence of dikes and high strain zones (moderately deformed protomylonite-mylonite). Gabbronorite dikes preferentially occur in the central parts of the high strain shear zones and in domains overprinted by the spaced serpentine cleavage. (Figure 5b) Small-sized cataclasites show two preferential orientations: N-S and NNW-SSE, while the large-scale cataclastic zones only display NNW-SSE directions (dark blue domains are mapped areas along Wadi al Wasit, while bright blue ones represent interpolations).

3. Results—Field Relations

3.1. Evidence for Magmatic Activity

In the harzburgite of Wadi al Wasit three major representatives of magmatic activity can be distinguished: (a) dunite bands, (b) websterite dikes, and (c) gabbronorite dikes (Figures 5a and 6–10).

1. Dunite bands provide the oldest evidence for magmatic activity. They occur in porphyroclastic peridotites and show N-S orientations but variable dip angles (Figure 9). The dunite bands reveal two distinct appearances. They occur in form of compositional bandings where few centimeter-thick dunite layers alternate with harzburgitic layers (Figure 6f). In some cases, arrays of dunitic bands form interconnected networks (Figure 6b). Alternatively, they appear as subvertical lozenge-shaped bodies (boudins) of 10–20 cm thickness (Figure 6a). These bodies are discordant to the layering of the harzburgite. Several centimeters large pyroxenes occur in the central part of the lozenges (Figure 6a), and the dunites usually show sharp contacts to the harzburgite.
2. Websterite dikes are genetically younger than the dunites as demonstrated by cross-cutting relationships. The websterites are often pegmatitic with several centimeter-long enstatite and diopside (Figures 6c–6f). Different generations of pyroxene suggest multiple injection events, i.e., fracturing-crystallization cycles (Figure 6d). The thickness of websterite dikes varies between < 2 cm (wb 1), 2–20 cm (wb 2), and > 20 cm (wb 3). In a few cases, websterites show homogeneous grayish appearance suggesting grain sizes < 1 mm (wb 4). Occasionally, the websterite dikes are folded (Figure 6e). The magmatic textures are partially overprinted by solid-state deformation as illustrated by strain localization associated with grain size reduction at the harzburgite-websterite interfaces or by boudinage of the websterites within the viscous harzburgite matrix (Figure 6f; see also Figure 16b in *Herwegh et al*. [2011]). Primary diopside and enstatite display mutual exsolution lamellae of the complementary pyroxene. In domains of ductile overprint and/or boudinage, the deformation twins can be bent (Figure 7a) and the former large-sized pyroxenes undergo grain size reduction. The latter occurs by a combination of dynamic recrystallization and nucleation of new grains leading to the formation of a second generation of recrystallized pyroxenes with smaller grain sizes compared to their parents (Figure 7a). Toward the main shear zone, some websterites (wb 5) show

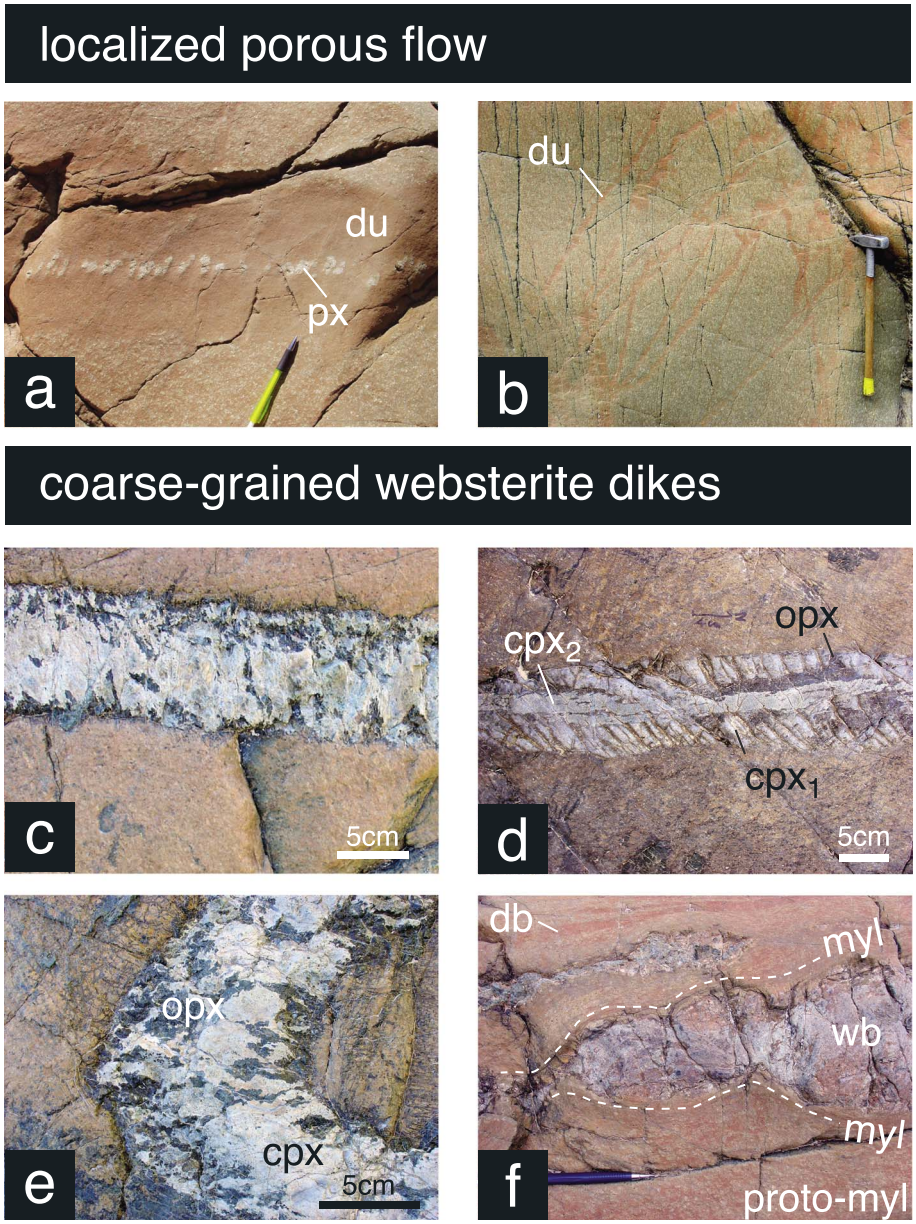

Figure 6. Field photographs of dikes emplaced in the harzburgite. Indications for localized porous flow: (a) reactive veins with isolated aligned pyroxene grains in the center of a dunite (du) band (detail out of a lozenge-shaped body) and (b) interconnected network of dunite bands represent former pathways of melt in the harzburgitic host rock, where only the reaction products were left and the melt migrated upward into shallower levels of the lithosphere. (c) Coarse-grained websterite dikes (type wb 2, see text) consisting of enstatite and diopside show fibrous growth; (d) multiple opening and growth stages (cpx_1 and cpx_2, generations), and (e) overprint by folding is frequent. (f) Boudinage of websterite (wb) dike, with dramatic grain size reduction from protomylonite (proto-myl) to the mylonite (myl) along the websterite contact indicating strain localization along this interface. Note also the changes in foliation from protomylonite-dunite (db) banding to mylonite.

minor amounts of plagioclase along fractures, cleavage planes, and between grain boundaries of orthopyroxene (opx) and clinopyroxene (cpx) (Figure 7b).

3. The gabbronorites represent the youngest dike generation in Wadi al Wasit; i.e., they either crosscut both dunitic bands and websterites (Figures 8e and 8f) or reactivate websterite dikes (Figure 8d). They are pegmatitic and consist of large centimeter-sized diopside and enstatite surrounded by interstitial plagioclase

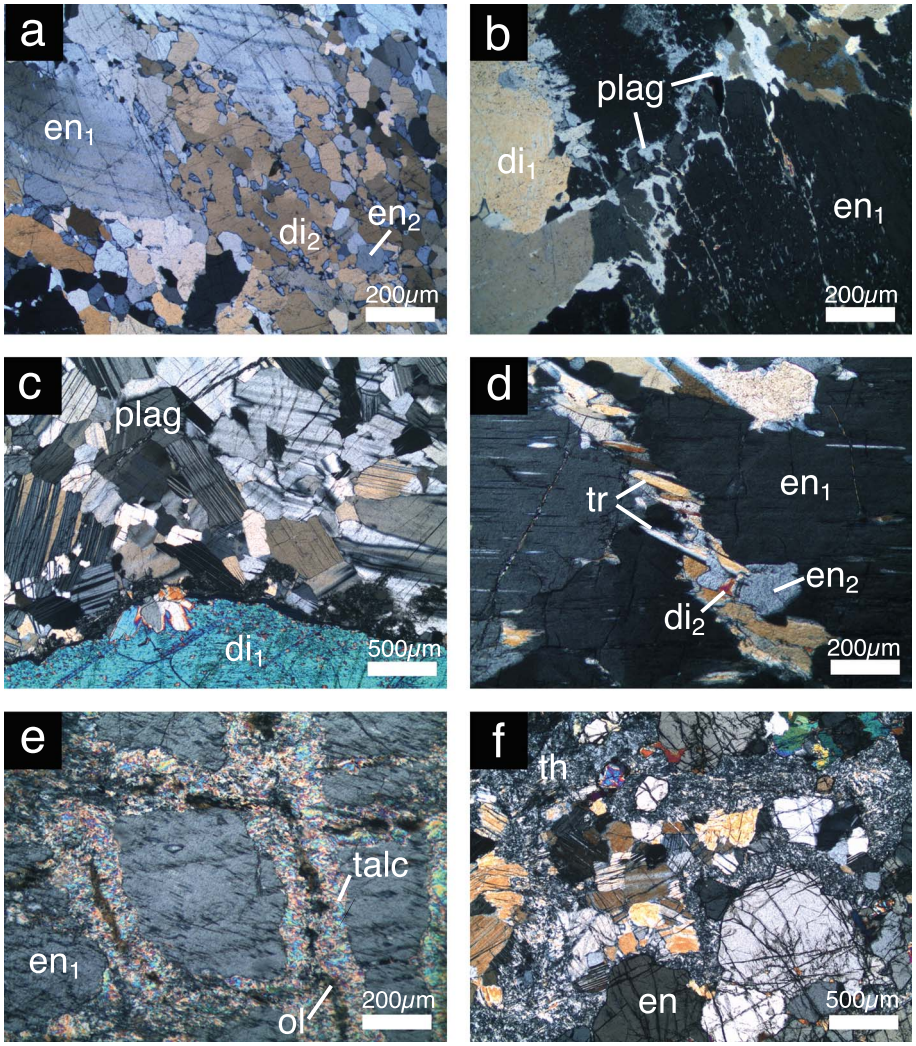

Figure 7. Microstructures in dikes. (a) Websterite dike consisting of original large-sized magmatic enstatite (en1) with bent twins indicating intracrystalline plasticity. Enstatite grain (en1) recrystallizes into small-sized crystallization diopside (di2) and enstatite (en2) as recrystallization products. (b) Plagioclase bearing websterite dike with large-sized magmatic enstatite (en1) and diopside (di1) become infiltrated along the grain boundaries by melt as indicated by plagioclase (plag) as remnant. (c) Gabbronorite with fine-recrystallized plagioclase suggesting dynamic recrystallization during solid-state viscous deformation. (d) Coarse-grained magmatic enstatite (en1) becomes fractured during deformation resulting in recrystallization of enstatite (en2), diopside (di2) and tremolite (tr) in the dilatant domain of a websterite dike. Appearance of tremolite is the first indicator for the presence of a hydrous phase. (e) Low-temperature fracturing of enstatite (en1) in websterite under hydrous conditions resulting in talc and olivine (ol) as reaction products. (f) Further low-temperature alterations of gabbronorites in the presence of fluids lead to thomsonite (th), which replaces the former plagioclase.

(Figure 8a). Plagioclase also locally exists either interstitially between medium-sized pyroxene grains or as patchy accumulations in the harzburgite (Figures 8b and 8c).

Gabbronorite dikes are neither folded nor boudinaged. In many cases, the gabbronorites follow the traces of preexisting websterite dikes using the preexisting mechanical anisotropy for melt injection. When isolated within harzburgite, one interface of the gabbronorites often shows the irregular geometry typical for injection phenomena like small apophyses, while the other boundary is always sharp and straight (Figure 8f). In other cases, gabbronorite-harzburgite contacts are very sharp, with a strong foliation over few centimeters on the gabbronorite site. The grain size of the plagioclase along the boundary is reduced relative to the much larger pyroxenes (Figure 7c), and a well-defined foliation exists. These zones reflect local shear zones along the gabbronorite-harzburgite interfaces. Note that neither websterites nor gabbronorites contain magmatic

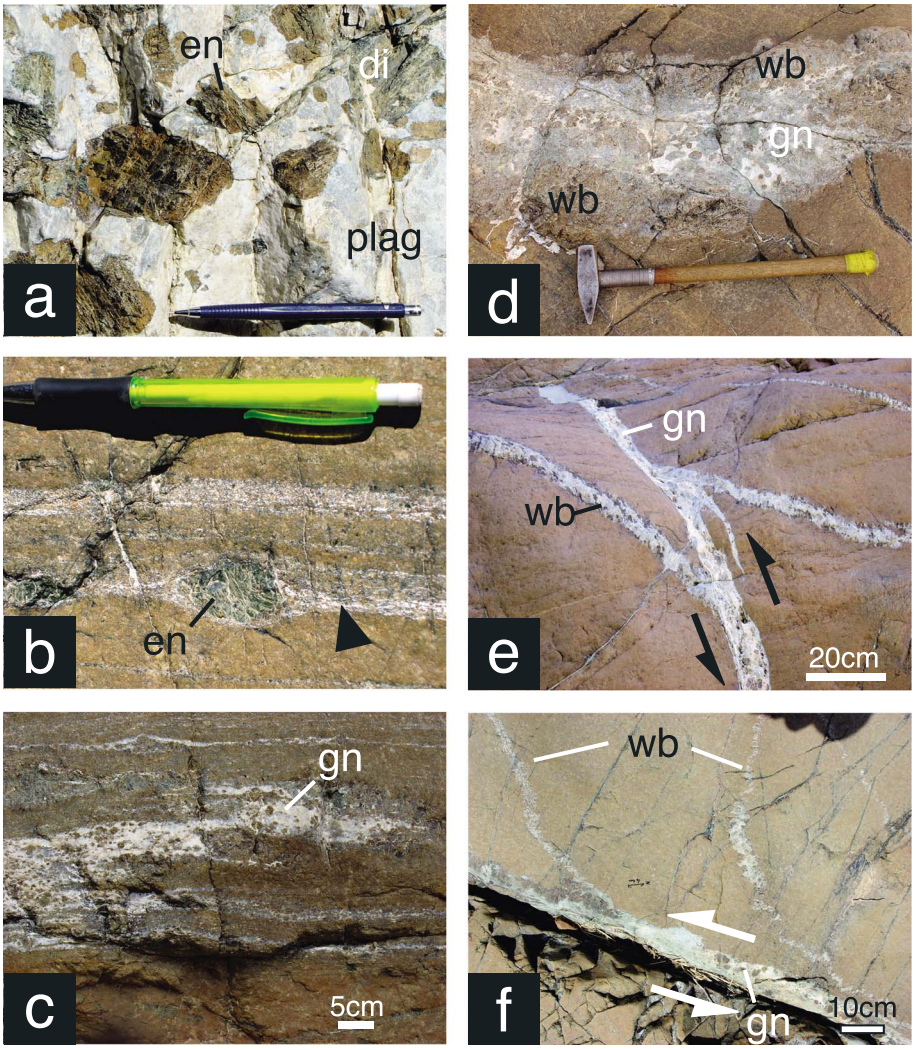

Figure 8. Photographs presenting gabbronorite dikes and their different deformation structures. (a) Internally undeformed pegmatitic gabbronorite with large-sized enstatite (en), diopside (di) and plagioclase (plag) grains. (b) Bands of small-sized pyroxenes with interstitial plagioclase (white) as indicators of melt impregnation during high-temperature deformation of the harzburgite and (c) melt pockets in form of accumulated plagioclase (white)-pyroxene aggregates. The occurrence of the large enstatite grain in Figure 8b gives a minimum width estimate of the former dike, where filter pressing of the melt induced exfiltration and thinning of the dike. (d) Reactivation of old websterite (wb) dike by fracturing and injection of gabbronoritic (gn) melt in the center. (e) Cross-cutting relationships as well as (f) dragging of websterite dikes into gabbronorite demonstrate a younger age of the gabbronorite (gn). (Figure 8f) The gabbronorite shear zone is reactivated again at a late stage by brittle deformation.

amphiboles as observed at different sites of the second magmatic suite [*Python and Ceuleneer*, 2003; *Boudier et al*., 2000].

Despite being all N-S oriented (Figure 5a), characteristic differences exist in terms of dipping angle of the dikes in the different host rocks (Figure 9). While dunites and websterites occur from vertical to almost horizontal orientations in the porphyroclastic harzburgite, they tend to become oriented vertically in weakly to moderately deformed protomylonites and are strictly vertical in the mylonites. Moreover, plagioclase bearing websterites and gabbronorites are only found in protomylonites and mylonites and are always vertical (Figures 9b and 9c).

In a cross section of the shear zone, both gabbronorite and websterite dikes show highest concentrations by volume and number of dikes close to the center of the major shear zone (Figure 10). Note that the apparent lack of dunite bands in the shear zone center might reflect an artifact related to the difficulty

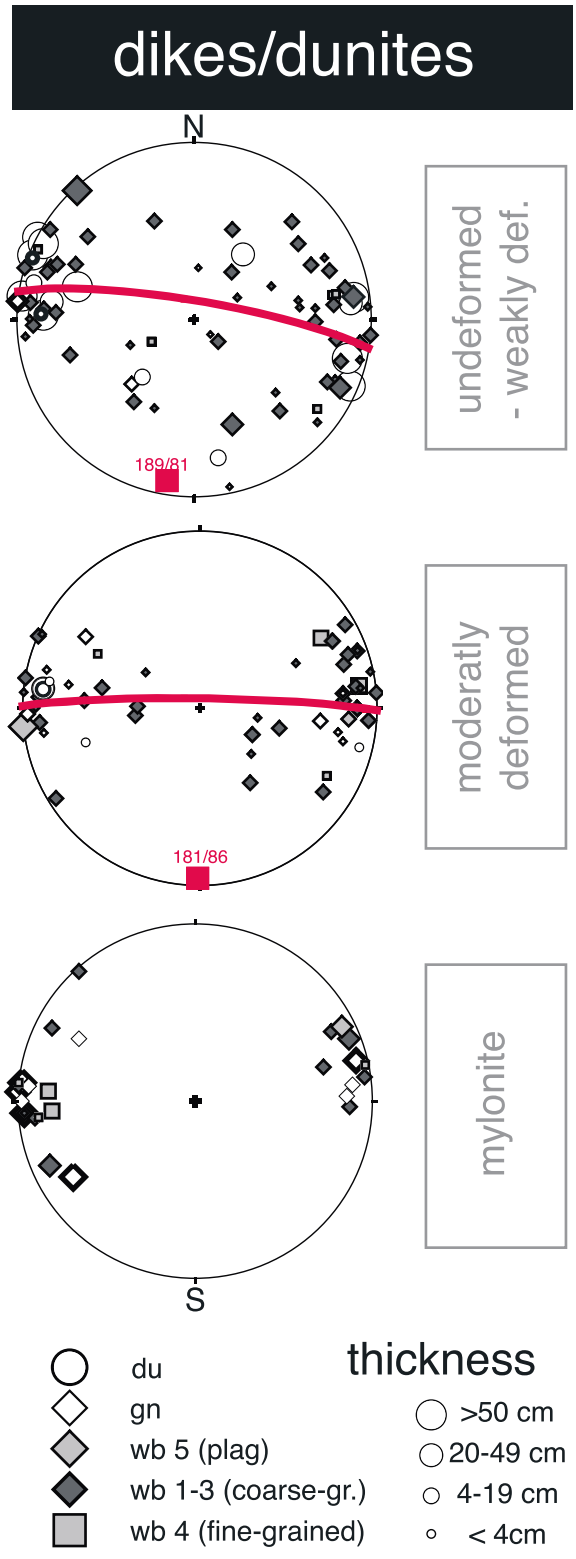

of the discrimination of fine-grained polymineralic mylonites from dunitic mylonites on a macroscopic scale. Due to the lack of large-sized pyroxene clasts and severe surface weathering the two types have similar macroscopic appearance.

3.2. Retrograde Mineral Assemblages and Late Brittle Overprint

Retrograde (hydrous) mineral assemblages are important proxies for the detection of potential influx of fluids into the mantle. Dikes are of particular significance as they can serve as potential fluid pathways. The very rare occurrence of tremolite in websterite dikes reflects the first evidence for hydrous phases in the mantle rocks of Wadi al Wasit (Figure 7d). The few small grains of tremolite occur as overgrowths along tensile fractures in pyroxenes together with newly precipitated fine-grained diopside and enstatite (Figure 7d). In some cases, tremolite appears along cleavage planes of the large old enstatite grains.

A second rare hydrous mineral found in fractured magmatic enstatite is talc. It forms via the reaction enstatite + H_2O = talc + olivine in fractures with talc at the rim and olivine in the center (Figure 7e). In ultramafic compositions at low pressures, talc is stable between 700 and 500°C [*Ulmer and Trommsdorff*, 1999], or alternatively, it forms at the expense of opx by infiltrating Si-rich fluids beneath the seafloor [e.g., *Boschi et al.*, 2006].

The serpentine polymorph lizardite, as confirmed by few measurements using Raman spectroscopy, is the most abundant hydrous

Figure 9. Stereographic projection of dike orientations and dunite bands as a function of increasing shear strain (top-down) of the harzburgite. The original dike orientation can be inferred from the dikes in undeformed porphyroclastic fabrics and weakly deformed protomylonites. The initial dikes were N-S trending with various dipping angles rotating around a N-S trending axis (pole and great circle in red). Moderately deformed protomylonites still reflect dike orientations close to their initial injection, again with varying dipping angles around N-S oriented rotation axis. With increasing shear strain, the dikes keep their strike but rotate into parallelism with the vertical shear plane in the case of the mylonites. The symbol size correlates with the dike thickness. Abbreviations: dunite band (du), gabbronorite (gn), and websterite (wb).

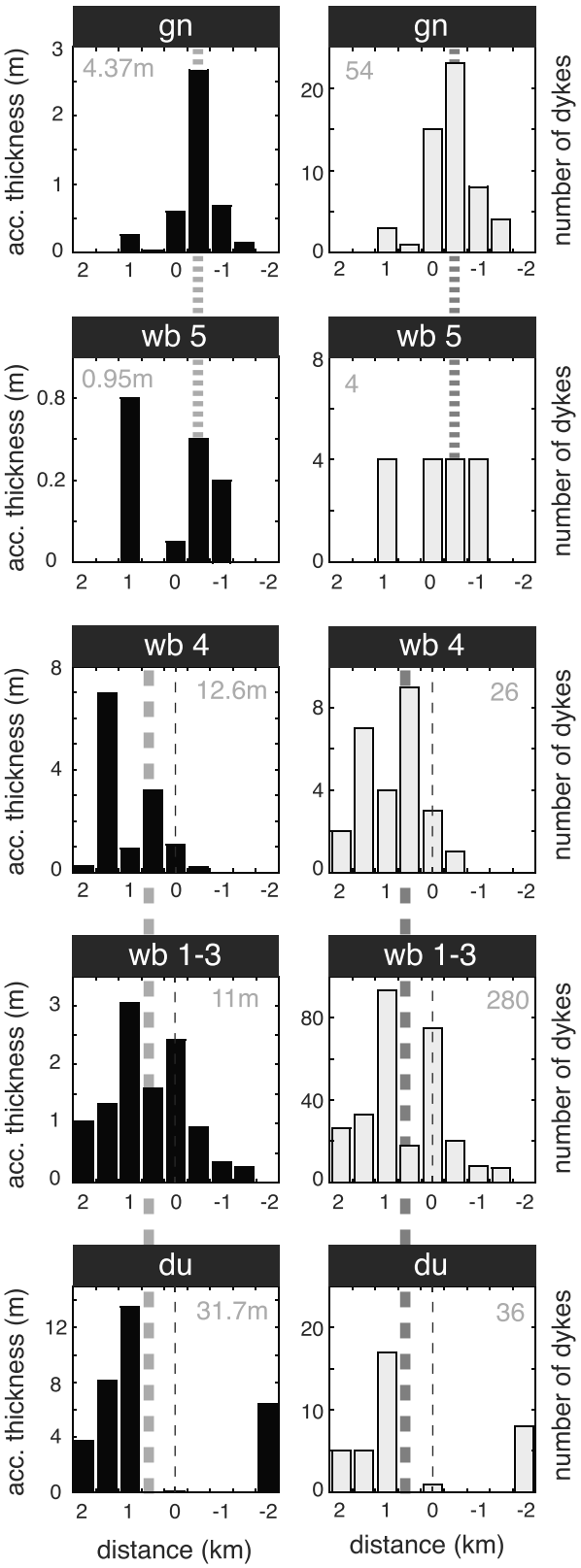

mineral found in the porphyroclastic to mylonitic harzburgite and in the dikes. Its first appearance in the harzburgite is restricted to the central part of the Wadi al Wasit shear zone, where a spaced cleavage of lizardite develops (Figure 2). This cleavage strikes NNE-SSW and is subvertical. It is overprinted by cataclastic zones of various dimensions (few millimeters up to hundred meters) and orientations ranging from N-S and NW-SE (Figure 5), while the large-scale cataclasites are oriented NW-SE (Figures 2 and 5b). The entire mantle rocks thus show a complex brittle fragmentation. Between the brittle faults, lizardite appears in typical mesh textures, and its content varies from 20 to 100 vol %. Generally, serpentine abundance rises with increasing degree of brittle overprint. The zeolite thomsonite (Figure 7f), replacing plagioclase in the gabbronorites, is the lowest-grade hydrous mineral (temperatures 150–275°C, *Joan and Lo* [1969] and *Wirsching* [1981]) overprinting the rocks in Wadi al Wasit.

4. Discussion

In the Wadi al Wasit shear zone, the continuous succession from ridge-related asthenospheric flow via melt-assisted to solid-state deformation, to final brittle behavior, represents an excellent opportunity to study strain localization and associated rheological and geometric constraints with progressive cooling of harzburgitic mantle (Figures 11–14).

Figure 10. Histograms showing (left column) accumulated thickness and (right column) number of dikes collected in intervals of 500 m in a profile across the main shear zone in Wadi al Wasit. Zero corresponds to the shear zone center (thin stippled line) and positive and negative values to west and east direction. Note the correlation between peak of accumulations and the shear zone center for websterites (wb 1–4) and gabbronorites (gn); wb 1–3: coarse-grained websterite dikes with dike thicknesses < 2 cm (wb 1), 2–20 cm (wb 2), and > 20 cm (wb 3); wb 4: fine-grained websterites; wb 5 websterite dikes with small volume fraction of interstitial plagioclase; du: dunitic bands. In Figures 10 (left column) and 10 (right column) the grey numbers in the graphs indicate the total accumulated thickness and total number of dikes, respectively. Note the change in location of the modes of the distribution (thick stippled lines) of the dikes from left (du, wb 1–4) to right side (wb 5, gn) of the shear zone center.

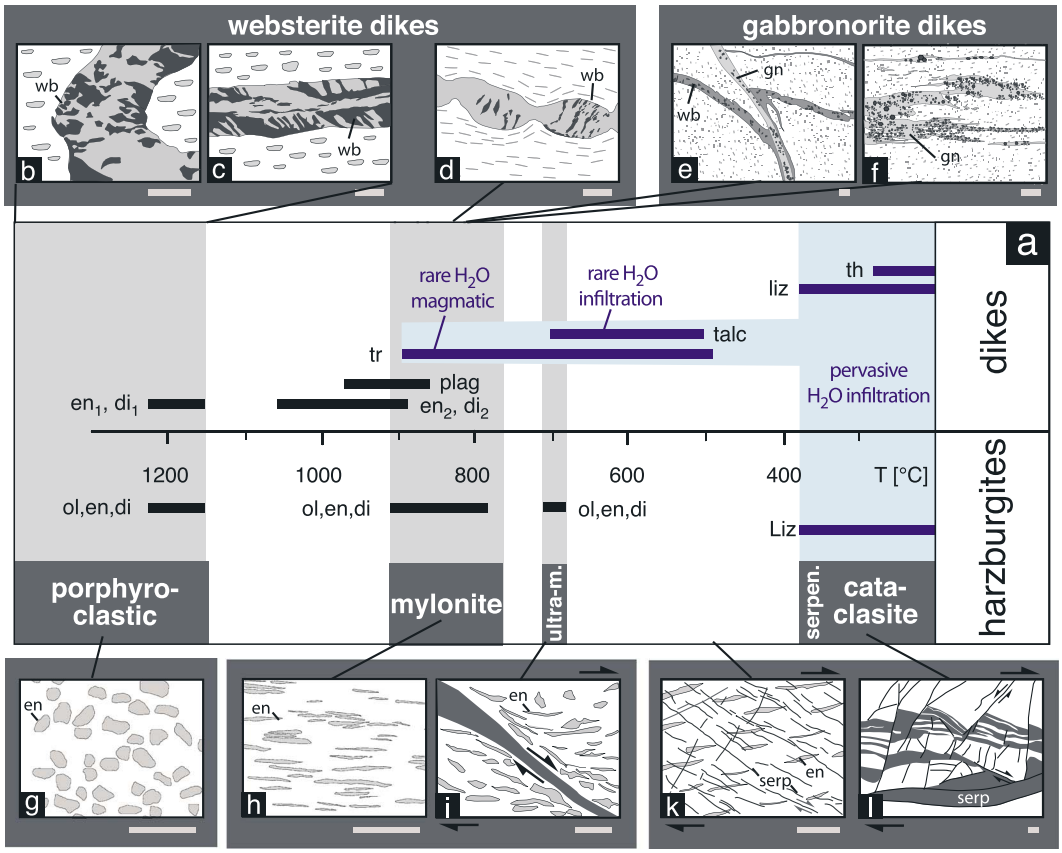

Figure 11. Correlation between evolution of the (g–l) different harzburgite tectonites and (b–f) magmatic dikes with (a) temperature and corresponding mineral stabilities. Old folded websterite (wb) dikes (Figure 11b) are found in porphyroclastic harzburgite (Figure 11g), with enstatite and diopside as major minerals in the dikes and additional olivine for the harzburgite (Figure 11a). With progressive cooling, solid-state deformation (900–800°C) in the mylonitic harzburgite (Figure 11h) leads to boudinage of the websterites (Figure 11d) accompanied by dynamic recrystallization of olivine in the mylonites as well as of enstatite and diopside in the case of the dikes. Tremolite in websterites represents first indications for hydration. Around 700°C the formation of ultramylonites indicates a last stage of ductile deformation and represents the onset of dominance in brittle deformation. Major fluid influx appears during brittle deformation below 400°C when in a first stage the spaced lizardite cleavage (Figure 11k) develops followed by the pervasive fragmentation of the ophiolite by cataclasites (Figure 11l) during obduction. Serpentinization (serp) of the harzburgite and the replacement of plagioclase by thomsonite indicate a major compositional and rheological change in the mantle sequence during low-temperature deformation and hydration. Ol: olivine, en: enstatite, di: diopside, plag: plagioclase, tr: tremolite, th: thomsonite, liz: lizardite.

Strain localization in the upper mantle is an important process for understanding initial rifting at mid-ocean ridges [*Buck et al.*, 2005; *Choi et al.*, 2008], development of mantle windows in magma-poor passive margins [e.g., *Müntener et al.*, 2000], the onset of suprasubduction zone spreading centers [*Rioux et al.*, 2012, 2013], or the lubrication of plate boundaries [*Holtzman and Kendall*, 2010].

In Wadi al Wasit it is evident that melt impregnation, dike injections, their spatial distributions and the parallel strike-slip movements must be closely linked with each other. In light of a correlation of the three major representatives of magmatic activity (Figures 6–8) with previous studies we emphasize that websterite dikes and gabbronorite dikes exclusively represent the depleted suite of *Python and Ceuleneer* [2003], while the diapir-related features of the MORB suite are probably restricted to dunite channels. Hence, we can investigate the effect and interplay of the magmatic activity of the depleted suite on deformation in the Wadi al Wasit shear zone. In the following, we will discuss the relative timing and the thermomechanical implications for strain localization including the role of magmatic activity and magmatic precursors (Figures 11 and 12). Only 0.25–0.5 Ma separate the MORB dominated and the depleted magmatic activity [*Rioux et al.*, 2013]. No longer than 1.5 Ma later started the detachment of the lithospheric block (formation of the HT

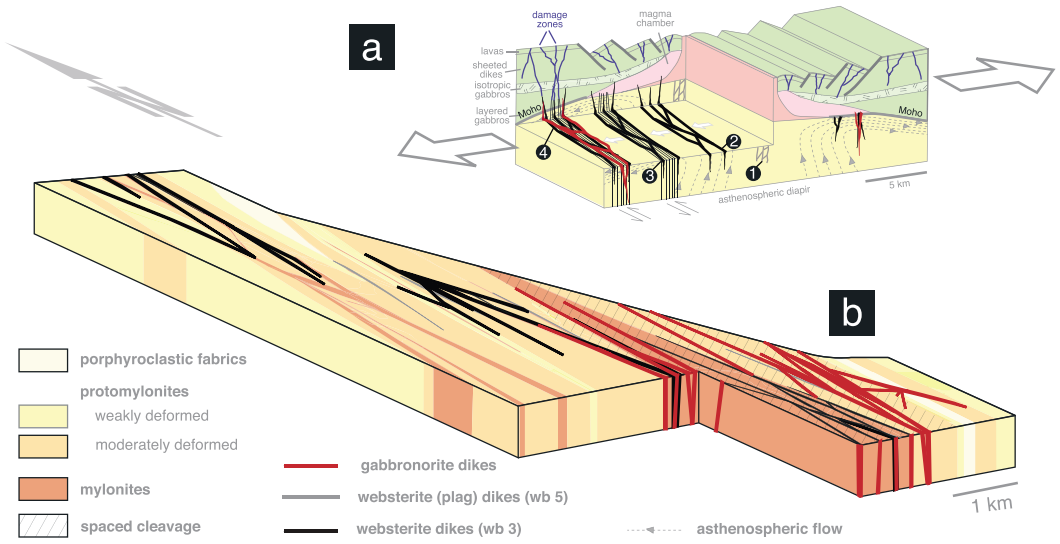

Figure 12. Schematic block diagram showing the evolution of the different structures with respect to (a) the spreading center (upper right corner) and (b) the enlarged situation in the Wadi al Wasit shear zone. Note that the latter represents the 3-D view of the map of Figure 2, now showing the extrapolated successions of the different dikes. Close to the ridge, an early stage of melt migration (asthenospheric flow) is manifest by dunite bands (1). Injection of early websterite dikes (2) close to the ridge control strain localization in the following deformation stages (3). With progressive spreading and cooling, episodes of ductile strike slip and magma injection take place (3). With the progressive cooling the crustal entrapment level of the gabbronorites decreases until these dikes are stuck at the level of the now exposed Wadi al Wasit (4), i.e., at farther distance to the spreading center.

metamorphic sole) [*Warren et al*., 2005; *Rioux et al*., 2012, 2013]. Therefore, the sequence of ductile deformation styles (protomylonites-mylonites-ultramylonites) must have developed in a very short time interval. To unravel the formation of mechanical anisotropies and their reactivation in subsequent deformation stages, we start discussing the structures formed early and progress then to subsequent deformation stages.

4.1. Early Ridge-Related High-Temperature Structures

Although found in the eastern part of the Hilti massif [*Boudier et al*., 1988; *Ceuleneer et al*., 1988; *Nicolas et al*., 1988], equidimensional coarse-grained fabrics typical for early ridge-related flow have not survived in Wadi al Wasit because of their transposition into the porphyroclastic fabrics during subsequent deformation. Porphyroclastic fabrics are characteristic for high-temperature deformation at 1200–1100°C [e.g., *Dijkstra et al*., 2002; *Linckens et al*., 2011a] and evolved under solid-state conditions allowing for crystal plastic deformation in olivine [*Mercier and Nicolas*, 1975; *Ceuleneer et al*., 1988]. The flow stresses of solid-state deformation of the harzburgite were very low (Figure 14). At these conditions, olivine (1200°C: 1–3 MPa; 1100°C: 2–8 MPa using olivine flow laws of *Hirth and Kohlstedt* [2003]) was slightly weaker compared to the pyroxenes (1200°C: 3–20 MPa; 1100°C: 8–45 MPa based on a flow law of *Dimanov and Dresen* [2005]), and both minerals were deforming by dislocation creep as confirmed by strong CPOs and the presence of dynamic recrystallization processes [e.g., *Michibayashi and Mainprice*, 2004; *Linckens et al*., 2011b].

Despite being rarely preserved in the studied area (Figures 2 and 12), the porphyroclastic fabrics are important, because they contain the oldest dike generations not affected by strike-slip shearing (see 1 in Figure 12a). Typically, early websterite dikes and dunite bands are representatives of such early melt extraction structures (Figure 11). As a result of variable dipping angles but constant N-S strike (Figures 6, 9, and 12) the best fit of their orientations defines a great circle in a stereographic projection (Figure 9, top). The pole of the great circle is subparallel to the ridge axis inferred from the sheeted dike complex of the oceanic crust (cf. Figures 1 and 12). Such a geometry correlates well with conjugate sets of fracture planes [see, e.g., *Weinberg and Regenauer-Lieb*, 2010, their Figure 3] related to the general stress field near a mid-ocean ridge with σ_1, σ_2, and σ_3 being vertical, horizontal-ridge parallel, and horizontal but perpendicular to the ridge, respectively [*Nicolas and Jackson*, 1982; *Nicolas et al*., 2000]. These inferences combined with the observation

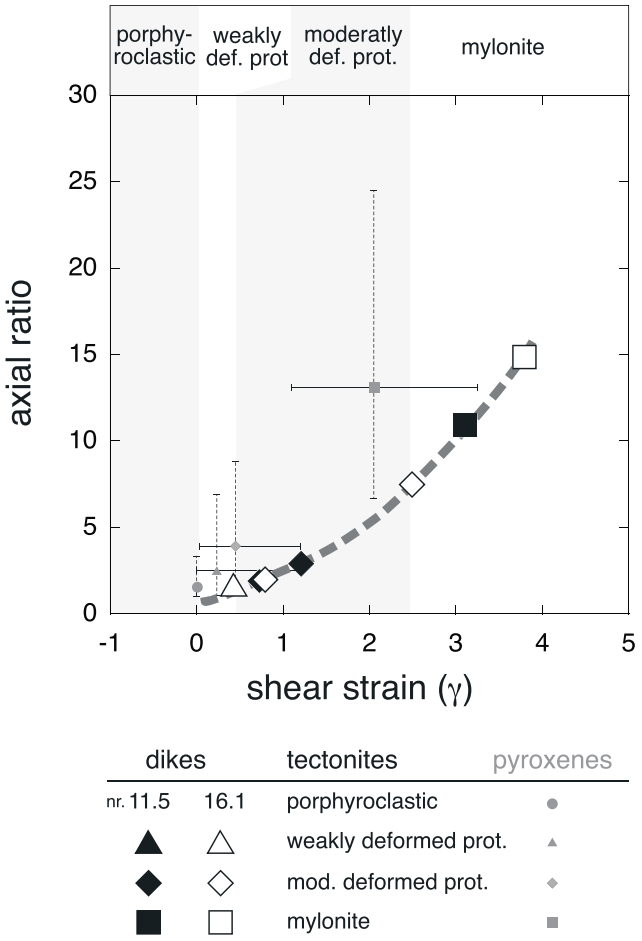

Figure 13. Diagram displaying the correlation of the four major tectonites to finite strain. Finite strain is estimated by axial ratios of pyroxenes (grey symbols) and two sheared websterite dikes (sample11.5 and sample16.1). In the case of the dikes, strain ellipses were calculated on the base of the measured shear strain. Grey bars of the axial ratios of pyroxenes represent minimum and maximum axial ratios of the measured samples.

that most of the websterite and dunite bands are subvertical indicate that a vertically oriented compositional anisotropy evolved due to hydraulic fracturing or ductile shearing [see also *Rybacki et al.*, 2010; *Weinberg and Regenauer-Lieb*, 2010] and melt injection close to the spreading center before the onset of ductile strike-slip shearing (Figure 12).

4.2. Strain Localization During Strike-Slip Shearing

Strike-slip shearing, as indicated by the transition from protomylonites to mylonites (Figures 1, 4, and 12), is the first evidence for strain focusing under solid-state deformation conditions in the Semail ophiolite [*Boudier and Nicolas*, 1985; *Boudier et al.*, 1988; *Ceuleneer et al.*, 1988; *Dijkstra et al.*, 2002; *Michibayashi and Mainprice*, 2004; *Michibayashi et al.*, 2006; *Linckens et al.*, 2011b; *Linckens et al.*, 2015]. Strain estimates for the Wadi al Wasit shear zone were generated by analyzing the grain aspect ratios of pyroxenes as well as passively sheared websterite dikes (see Figure 13 and above). Continuous elongation of pyroxene with increasing shearing suggest shear strains of 0.2–0.4 and 2–3 for the transition from weakly to moderately deformed protomylonites and from moderately deformed protomylonites to mylonites, respectively. Note that these values reflect minimum estimates since the viscous olivine matrix might have accommodated more strain than the less viscous pyroxenes. Additionally, minimum shear strains of 3–4 have been calculated for websterite dikes being dragged into mylonites (Figures 8f and 13). Extrapolated to the 500 m wide central part of the large-scale shear zone, an accommodation of at least 2 km of horizontal strike-slip displacement can therefore be postulated. Taking the time interval of 0.25–0.5 Ma for the activity of first ridge-related and the second suprasubduction zone-related magmatism [*Rioux et al.*, 2012, 2013] strain rates higher than $5 \times 10^{-13}\,s^{-1}$ must be assumed for the solid-state deformation of the Wadi al Wasit shear zone. We therefore assume strain rates of 10^{-12} to $10^{-13}\,s^{-1}$ as realistic [see also *Linckens et al.*, 2011b].

In the case of the Wadi al Wasit shear zone solid-state strike-slip shearing occurred at temperatures of 900–800°C (Figure 11 and *Linckens et al.* [2011a]). The dynamically recrystallized olivine grains, their elongated grain shapes as well as the strong olivine CPOs (in both monomineralic and polymineralic layers) indicate dislocation creep in monomineralic olivine aggregates as dominant deformation mechanism [*Linckens et al.*, 2011b]. Here rock strengths of 40–80 MPa and >220 MPa, respectively, can be inferred for olivine and pyroxenes (see Figure 14). Consequently, differences in effective viscosity between harzburgite and websterite dikes lead to the pronounced boudinage of the old websterite generations [*Herwegh et al.*, 2011, Figure 11d and their Figure 16b]. In contrast, parallel alternating polymineralic (ol, opx, and cpx) and monomineralic olivine layers in harzburgites are neither boudinaged nor fractured or folded (Figure 4) suggesting nearly equiviscous deformation [*Herwegh et al.*, 2011]. This similar rheological behavior is

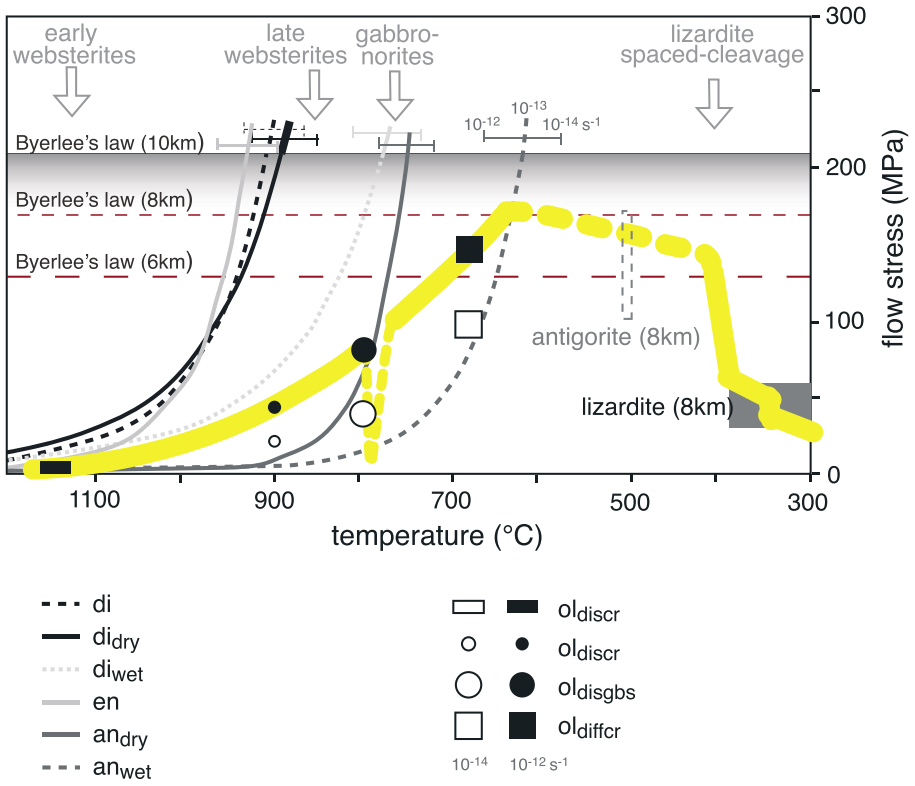

Figure 14. Rheological evolution (yellow line) with successive strain localization during progressive cooling of the mantle; 1150°C: Formation of dunite bands and injection of early websterite dikes under near-solidus conditions and low flow strengths; 900–800°C: increasing flow stress under dislocation creep conditions with progressive cooling and injection of late websterite dikes; 800°C: Deformation by dislocation accommodated grain boundary sliding, melt infiltration and injection of gabbronorite dikes. Note the near-equiviscous conditions for olivine and anorthite; 700°C: Termination of crystal plastic deformation of olivine forcing strain to localize in ultramylonitic polymineralic bands [see *Linckens et al*., 2011a, 2011b, 2015]. Further strike-slip shearing during cooling leads to embrittlement and infiltration of seawater forming the pervasive serpentine spaced-cleavage in the shear zone center (Figure 2). Formation of serpentine provokes a major drop in flow stress. Thin lines: extrapolated experimental flow laws for diopside (di: *Bystricky and Mackwell* [2001]; di_{dry}, di_{wet}: *Dimanov and Dresen* [2005]) enstatite (en: *Mackwell* [1991]), dry and wet anorthite (an_{dry}, an_{wet}: *Rybacki et al*. [2006]) where the error bars represent maximum, mean, and minimum strain rates of 10^{-12}, 10^{-13}, and 10^{-14} s^{-1}, respectively. Black solid and empty symbols flow laws of olivine (ol_{discr}): dislocation creep [*Hirth and Kohlstedt*, 2003]; (ol_{disgb}): dislocation creep accommodated grain boundary sliding [*Warren and Hirth*, 2006]; (ol_{diffcr}): diffusion creep of olivine [*Hirth and Kohlstedt*, 2003]). Grey stippled box: viscous frictional creep of antigorite [*Reinen et al*., 1994], grey filled box: viscous frictional creep of lizardite [*Reinen et al*., 1994; *Moore et al*., 1996]. Horizontal trends Byerlee's law at depths of 6, 8, and 10 km. Yellow: inferred evolution of bulk rheology of the shear zone with progressive cooling for a strain rate of 10^{-13} s^{-1} (black symbols); 10^{-14} s^{-1} (empty symbols). The presence of melt during interstitial melt migration of gabbronorites might have locally reduced flow stresses (thin stippled line).

attributed to olivine as volumetrically dominant phase forming interconnected weak layers in the polymineralic domains (Figures 4b–4e).

Strike-slip shearing was active at least till the formation of the ultramylonites, whose deformation temperatures were 700°C [*Linckens et al*., 2011a] and may even have continued to temperatures below 400°C, conditions at which the lizardite spaced cleavage evolved (see above, Figures 2, 11, and 12). In this broad temperature range, the processes responsible for strain localization may change, and we therefore will discuss them below as a function of retrograde cooling.

Strain localization occurs because of variations in effective viscosity between different rock volumes, where deformation tends to concentrate in the mechanically weaker rock [*Bowden*, 1970; *Hobbs et al*., 1990; *Mancktelow et al*., 2002]. For that reason, a variety of weakening processes in mantle rocks in general, and olivine in particular, have been studied in the past: (i) mechanical weakening of olivine by the presence of melt [e.g., *Nicolas et al*., 2000; *Braun and Kelemen*, 2002; *Dijkstra et al*., 2002; *Holtzman et al*., 2003a, 2003b;

Kaczmarek and Müntener, 2008; *Takei and Holtzman*, 2009] or (ii) water [*Hirth and Kohlstedt*, 1996; *Jung and Karato*, 2001; *Holtzman et al*., 2003a; *Renner et al*., 2003; *Katayama et al*., 2004; *Skemer et al*., 2013], (iii) changes in deformation mechanisms by the presence of second-phase minerals in a olivine dominated matrix promoting a transition from dislocation creep to diffusion creep [*Toy et al*., 2010; *Jaroslow et al*., 1996; *Newman et al*., 1999; *Dijkstra et al*., 2002; *Warren and Hirth*, 2006; *Linckens et al*., 2015], and (iv) the formation of CPO [*Michibayashi and Mainprice*, 2004; *Tommasi et al*., 2009; *Skemer et al*., 2013].

In the Wadi all Wasit shear zone all these strain-weakening effects, i.e., strain weakening by progressive microfabric evolution, inheritance of preexisting fabrics and activation of olivine low-temperature slip systems contributed to strain localization [*Linckens et al*., 2011a, 2011b; *Michibayashi and Mainprice*, 2004]. The role of water during ductile shearing remains unclear, however, since the few tremolites found in websterite dikes represent the only hydrous high-temperature minerals found. The extreme rarity of hydrous phases therefore clearly indicates the lack of large-scale, volumetrically significant, and pervasive infiltration of hydrothermal fluids before the beginning of the low-temperature crystallization of lizardite (see below). Yet we cannot exclude trace amounts of water in the olivine crystal lattice. We suggest that tremolite formed by the reaction of the magmatic pyroxenes with small amounts of H_2O, the latter probably being released by late stage fluid-saturated melt (Figure 11). All aforementioned strain-weakening processes could have occurred anywhere and spatially widely distributed, not explaining why deformation is concentrated along the exposed high strain zone.

We suggest that the mechanical anisotropies induced by dike intrusions represent the key feature for triggering the initial strain localization pattern (Figure 12). The folded and boudinaged websterite dikes clearly indicate enhanced solid-state rock strength compared to the more viscous harzburgite (Figures 6e, 6f, and 11). The extrapolation of experimental flow laws to deformation temperatures of 900–800°C and natural strain rates of $10^{-12}\,s^{-1}$ suggests flow stresses of the pyroxenes < 220 MPa, while olivine dominated fabrics yield flow stresses of 40–80 MPa (Figure 14, see also *Linckens et al.* [2011a]). The websterite dikes thus represent mechanically stiff inclusions in a viscous matrix. It is well known from numerical modeling that stress focuses at the edges of the inclusions, promoting strain localization at these sites [e.g., *Casey*, 1980; *Mancktelow et al*., 2002; *Wilson et al*., 2009]. In the Wadi al Wasit shear zone, evidence for strain localization induced by stress perturbations are indeed preserved in form of gradients in dynamically recrystallized grain size at the websterite-harzburgite contacts. Here coarse-grained host rock microstructures transfer to fine-grained mylonitic ones over distances of 1–30 cm (Figures 6f and 8f). On a larger scale, the enhanced dike density (Figure 10) therefore provides numerous sites for the nucleation of strain localization under solid-state conditions on the centimeter to meter scale. We suggest that shear zones nucleate on such stress perturbations [see also *Sengupta*, 1997; *Goodwin and Tikoff*, 2002; *Toy et al*., 2010], and the growth and interconnection of these embryonic mesoscale shear zones finally lead to strain localization on a regional scale resulting in the formation of shear zones such as the Wadi al Wasit shear zone (Figure 12).

4.3. The Role of Melt During Strike-Slip Shearing

Dunitic bands and websterite dikes are often discordant to the layering of the harzburgite. Several centimeter-sized pyroxenes occur in the central part of the lozenges of websterites (Figure 6a), and the dunites usually show sharp contacts to the harzburgite. Such structures were interpreted as zones of former localized porous flow underneath the mid-ocean ridge representing pathways for melts migrating upward into shallower mantle levels [e.g., *Kelemen et al*., 1995]. The boudinaged appearance of all websterites within these host rocks suggests either a preshearing or a synkinematic intrusive origin, which is confirmed by the widespread twinning of orthopyroxene in websterites (Figure 7a). In particular, coarse-grained dikes exceeding 50 cm thickness display no or only weak signs for internal deformation or boudinage at the outcrop scale, which we interpret as evidence for an injection during a late stage of strike-slip shearing. In any case, since no evidence for melt impregnation textures was found for the websterite dikes exposed in Wadi al Wasit, the segregation and collection of the melt of these websterite dikes must have been related to interconnection by porous flow at greater depths, eventually at the asthenosphere-lithosphere boundary [*Havlin et al*., 2013]. Consequently, hydrofracturing is the most probable emplacement mechanism of the websterite dikes [e.g., *Nicolas and Jackson*, 1982; *Havlin et al*., 2013; *Keller et al*., 2013]. In contrast, the occurrence of minor amounts of plagioclase along fractures, cleavage planes, and between grain boundaries of orthopyroxene (opx) and clinopyroxene (cpx) in some websterites located in the central part of Wadi al Wasit indicates the injection

of melt into the deforming websterite (Figure 7b). For the younger gabbronorites, pockets and layer-like domains of interstitial plagioclase in the harzburgite also indicate melt percolation at the grain scale (Figures 8b and 8c). These structures typically reflect zones of melt impregnation [*Dijkstra et al*., 2002], where melt is expelled by filter pressing with ongoing deformation (note the reduced width of the melt bearing zone as indicated by the large enstatite in Figure 8b) and becomes collected in melt pockets (Figure 8c). Such pools of collected melt may provide the sources for the injection of the gabbronorite dikes and the upward migration of the melt, a process called tectonic pumping [*Fyfe et al*., 1978]. Pinch and swell-like structures, with large pyroxene grains interconnected by thin planar bands of interstitial plagioclase (Figure 8b), suggest localized deformation in the presence of melt. Here compaction waves in combination with buoyancy might present the melt-migrating processes, as suggested, for example, by the numerical models of *Keller et al.* [2013]. Gabbronorites often follow the preexisting mechanical anisotropy at the contact between harzburgite and websterite by reactivating them as preferred injection sites. Solid-state deformation hardly affected the gabbronorites. Dry plagioclase, as volumetrically important phase of these dikes, has a much lower rock strength compared to olivine at temperatures above 800°C (see Figure 14). This strength contrast between olivine and plagioclase would promote strain localization and pervasive deformation of the gabbronorites, which is not the case. In contrast, their pegmatitic texture is perfectly preserved. Based on this observation and the occurrence of melt impregnation structures, we infer that injection of gabbronorites occurred during a late stage of mylonitic shearing where strain localization took place at deformation temperatures of about 800°C, i.e., under conditions where plagioclase and olivine were nearly equiviscous with flow stresses of 40–80 MPa (Figure 14). As mentioned above, however, some of the gabbronorite-harzburgite contacts show dramatic grain size reductions over few centimeters accompanied by mechanical twinning of plagioclase. We interpret these interfaces to be affected by extreme strain localization under solid-state conditions at a later stage of deformation. All these observations have important implications for the interpretation of the thermomechanical evolution of the shear zone at intermediate temperatures:

1. The rapid emplacement and associated cooling of the dikes during strike-slip shearing reflects ductile deformation interrupted locally by brittle fracturing and melt injection. Although the overall bulk strength of the shear zone was probably dominated by the solid-state rheology of olivine in the harzburgite, local melt impregnation via porous flow potentially temporarily reduced the rock strength [*Takei and Holtzman*, 2009; *Holtzman and Kendall*, 2010] leading to strain rate variations. The fastest deformation is most likely related to initial fracturing during dike emplacement. Two contrasting mechanical models could explain the buildup of pore pressure and magma fracturing. (i) The presence of melt and simultaneous buildup of pore fluid pressure results in hydraulic fracturing if the tensile yield strength is reached [e.g., *Nicolas and Jackson*, 1982; *Keller et al*., 2013]. (ii) The formation of ductile fractures [*Regenauer-Lieb*, 1999; *Weinberg and Regenauer-Lieb*, 2010]. In the latter model, solid-state deformation in the harzburgite induces the generation of pressure gradients and porosity. The polymineralic harzburgite, with their enhanced component of grain boundary sliding with increasing pyroxene content [*Linckens et al*., 2011b], would provide excellent sites for void formation and infiltration of melt. With progressive ductile deformation, the voids interconnect ending in bands filled with melt [see also *Keller et al*., 2013]. We suggest that in the Wadi al Wasit shear zone, the melt impregnation structures and associated melt pockets are best explained by the ductile fracture model (Figures 8b, 9b, and 9c), while large dikes suggest rapid injection by hydraulic fracturing (Figures 6c–6e). The latter cannot be excluded during ductile fracturing, particularly in cases where accelerated crack propagation may occur under the presence of interconnected melt [*Weinberg and Regenauer-Lieb*, 2010]. In any case, vertical fracturing additionally might be facilitated by the anisotropy of thermal expansion/contraction of olivine ($b > c > a$ axes, see *Boudier et al.* [2005]). Given the inherited orientation of olivine in porphyroclastic harzburgite, with the *a* axis parallel to the principal stretching direction σ_1, ridge parallel dilatancy would support the evolution of the vertical dike systems (Figure 15). This is probably only the case during the early stages of shearing because of reorientation of the olivine's *b* and *c* axes during mylonitization and the randomization of the CPO during ultramylonitic deformation [see *Linckens et al*., 2011b].
2. The transition from replacive dunite bands via websterite to gabbronorite represents a cooling sequence resulting from crystallization of melts at different ambient temperatures and/or a prominent change in melt source. The websterite-gabbronorite suite may have crystallized from a parental melt enriched in SiO_2 but depleted in incompatible elements (Na, Ti) and LREE clearly different than the MORB source affinity of the earlier dikes [*Boudier et al*., 2000; *Python and Ceuleneer*, 2003]. *Rioux et al.* [2012, 2013]

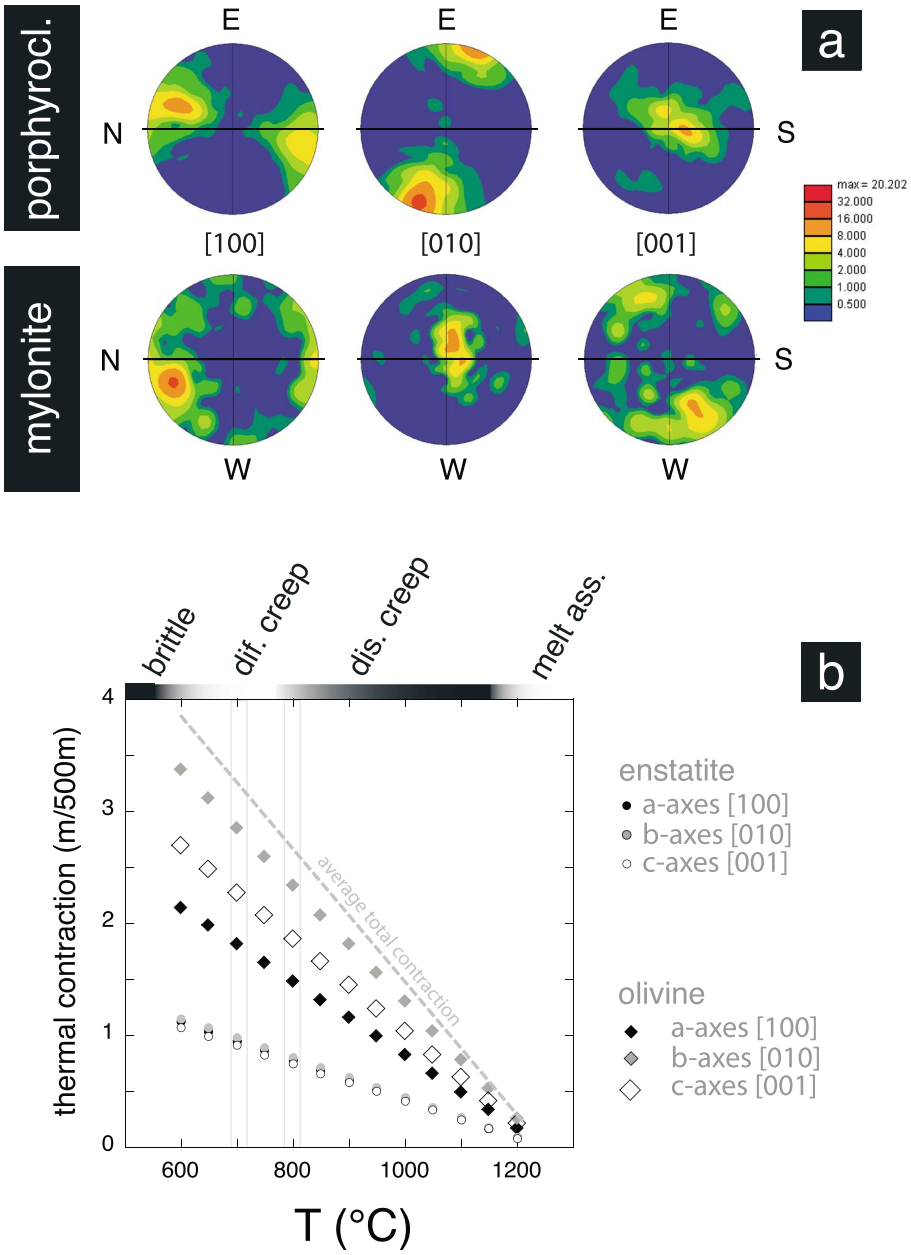

Figure 15. (a) Olivine CPO of *a*, *b*, and *c* axes for porphyroclastic and mylonitic microfabrics (data from *Linckens et al.* [2011b]) in their geographic reference frames (north, left). Note the inherited CPO of the porphyroclastic fabrics with the E-W alignment of the *b* axis. (b) Diagram displays changes in thermal contraction of olivine and enstatite along the different crystallographic axes during progressive cooling using thermal expansion coefficients given in *Boudier et al.* [2005]. Contraction is given in meters per intervals of 500 m across the shear zone. Note the anisotropic thermal contraction behavior of olivine with the following order: *b* axis > *c* axis > *a* axis, while enstatite is isotropically contracting.

suggested that this change reflects the onset of a suprasubduction environment of the ophiolite. However, gabbronorites have also been described from the fast-spreading East Pacific rise [*Gillis et al.*, 2014] where a suprasubduction environment can be excluded. The transition from websterites and gabbronorites was used as a qualitative paleodepth indicator in the mantle, an approach that was questioned by *Python and Ceuleneer* [2003] because both dike types were found at all lithospheric levels in Oman. Our new results from the dike sequence of the Wadi al Wasit shear zone provide an explanation for this apparent discrepancy. The replacive dunite bands represent the oldest remnants of former melt conduits close to or above temperatures of 1200°C (see Figures 7a and 7b and 1 in Figure 12a), the segregated melts

migrated upward to shallower lithospheric or crustal levels. Continuous strike-slip shearing, along with progressive spreading and associated cooling, resulted first in the emplacement of the websterite dikes in the temperature range from 1200 to 1100°C (Figures 11a–11e and 2 and 3 in Figure 12a). The harrisitic growth of the coarse-grained pyroxenes points to intrusion of the websterite dikes into already colder harzburgite favoring rapid cooling and crystallization (Figures 6c and 6d). The remaining melt migrated further upward and saturated in plagioclase in addition to pyroxenes promoting the formation of gabbronorites at temperatures below 1100°C (Figures 11e and 11f). Hence, the stages of melt trapping and crystallization correlates with a progressive cooling in space and time during ongoing strike-slip shearing (Figure 12). As a consequence, young gabbronorites are juxtaposed to older websterites because they become stuck at the same but now colder lithospheric levels (see 3 and 4 in Figure 12a). The same behavior holds for an earlier cooling stage for the association websterite-dunites (1 and 2 in Figure 12a). In this way, the dike sequence reflects the cooling pattern of the upper mantle, i.e., the distance from the ridge. Thus, the lithospheric level in which the dikes became stuck strongly depends on the thermal structure of the local lithosphere at the time of injection (Figure 12). In addition, if the websterite-gabbronorite suite indeed represents a crystallization sequence of more depleted magmas, the tectonic regime has probably changed as a consequence of suprasubduction spreading.

3. The final intriguing aspect is the ridge-parallel spatial concentration of dunite bands, websterite, and gabbronorite dikes (Figures 6 and 12) across the Wadi al Wasit shear zone (Figure 10). The width of these distributions decreases along the sequence dunites-websterites-gabbronorites (Figure 10). This distribution might be explained in two ways: (i) strain localization and associated shear zone narrowing with decreasing temperature and (ii) the dike interaction process discovered by *Ito and Martel* [2002]. (i) In a solid-state material deforming at colder temperatures, more energy is used to maintain viscous deformation processes per unit volume. Given a constant amount of deformation energy, dissipation over a smaller rock volume during cooling results in shear zone narrowing [e.g., *Ebert et al*., 2007]. Since hydrofracturing is restricted to the active shear zone, the area in which dike injection can occur narrows with decreasing temperature. Along with aforementioned changes in crystallization temperature of the melt, this behavior results in a dike sequence as a function of decreasing shear zone width. (ii) For the dike interaction process of *Ito and Martel* [2002], newly intruding dikes become focused by the remote stress fields induced by previously emplaced and crystallized dikes. A prerequisite for this process is a minimum spacing of the dikes, i.e., at maximum distances of 3–6 times the dikes head lengths [*Ito and Martel*, 2002]. For multiple dike injections in a vertical mantle section, a pyramid-shaped envelope of the dike population evolves, with a large number of spatially separated dikes at its base and few closely spaced dikes at its tip [see *Ito and Martel*, 2002, their Figure 8]. Since the possible interaction distance between dikes decreases with increasing remote stresses, i.e., with increasing viscosity, the progressive cooling of the harzburgite would result in a narrowing of the tip of the dike interaction pyramid at deeper levels. This behavior, combined with faster crystallization of dikes intruding into the colder mantle, can also explain the narrowing of the distribution from dunite bands over websterite to gabbronorite dikes in Wadi al Wasit (Figure 11). The two processes (i) and (ii) can be considered as end-members, which in fact might be simultaneously acting. In this way, progressive cooling does not only localizes solid-state deformation but also localizes dike intrusions. Hence, a positive feedback between ductile strain localization and dike emplacement evolves, both resulting in highly localized melt pathways and localized solid-state deformation of the harzburgitic host rock.

4.4. The Low-Temperature End of Shear Zone Activity

With respect to the harzburgitic host rocks, late strain localization is found in very fine grained ultramylonites, which are located within the mylonites [*Boudier et al*., 1988; *Michibayashi and Mainprice*, 2004; *Michibayashi et al*., 2006; *Linckens et al*., 2011a, 2011b]. Flow stresses in the range of 100–150 MPa can be expected for this last stage of viscous shearing before embrittlement and deformation following Byerlee's rule (Figure 14). Similar to feldspar dominated gabbronorites, the harzburgitic ultramylonites are concentrated in the center of the large-scale shear zone. The lack of both melt indicators and absence of hydrous minerals indicates that this deformation stage occurred without both melt and significant amounts of H_2O.

With ongoing cooling and hydrothermal overprint a lizardite serpentine foliation testifies for the onset of brittle deformation in the center of the shear zone (Figures 2, 12 and 14). At this stage, reactivation of the

preexisting mechanical anisotropies in the harzburgitic mylonites under the same overall stress field facilitates the access of H_2O-rich fluids in the central part of the former shear zone for the very first time in the history of the Wadi al Wasit shear zone (Figure 5). This clearly demonstrates the close link between brittle deformation, increasing permeability and the infiltration of fluids at temperatures below 600°C [*Boudier et al*., 2010]. The appearance of serpentine reduces the mechanical strength of the fault rocks to 30–50 MPa between 400 and 300°C (Figure 14). A definite change in the stress field is documented by the development of a cataclastic network of fault zones (Figures 2 and 5b). Here the initial shear zone is only partly reactivated, and it is the first time in the entire evolution in Wadi al Wasit that new, dike-independent orientations of fault rocks appear, resulting in a fragmentation of the entire mantle sequence (Figure 5b). Due to west directed emplacement of the ophiolite sequence onto the Arabian shield, a new set of WNW-ESE trending large-scale cataclastic fault zones develop, which dissect the former N-S trending mantle shear zone.

4.5. The Wadi al Wasit Shear Zone in Comparison to Other Mantle Shear Zones

Strain localization in the upper mantle is basically expressed in two different types of fault zones: (i) low-angle extensional detachment faults and (ii) transform faults (see reviews of *Vauchez et al*. [2012] and *Tommasi and Vauchez* [2015] and references therein). A review of the available literature indicates that (i) is more prominently presented. From a mechanical and kinematic point of view, however, the Wadi al Wasit shear zone clearly belongs into group (ii), although never having experienced a classical ridge perpendicular transform setting. Despite geodynamic and kinematic differences, (i) and (ii) both share a common thermomechanical evolution. For example, strain localization mostly starts with an early high-temperature deformation (porphyroclastic fabrics) associated with synkinematic melt migration (e.g., Beni Bousera: *Frets et al*. [2014]; Lanzo: *Kaczmarek and Müntener* [2008, 2010] and *Kaczmarek and Tommasi* [2011]; Othris: *Dijkstra et al*. [2004]; Lizard ophiolite; *Allerton and Macleod* [1998]; and Josephine: *Kelemen and Dick* [1995]), suggesting deformation in the vicinity of a thermal anomaly [*Vauchez et al*., 2012], a hypothesis which has recently been supported by geophysical surveys using SKS-wave splitting in the active rift setting of the Afar (Ethiopia) region [*Hammond et al*., 2014]. As shown by experimental investigations, the presence of melt reduces the harzburgite's flow strength [*Hirth and Kohlstedt*, 2003; *Zimmerman and Kohlstedt*, 2004] forcing deformation to localize. The chicken-or-egg question is whether the presence of melt is required to promote strain localization [*Holtzman et al*., 2003a, 2003b] or whether solid-state deformation provides the sites for melting [see *Vauchez et al*., 2012]. The Wadi al Wasit shear zone may provide some new insights. Due to the subvertical nature of the Wadi al Wasit shear zone, we infer that buoyancy-driven upward migration of melt is more efficient compared to aforementioned low-angle extensional scenarios with melt migration focusing along shallowly dipping shear planes. During the earliest magmatic activity, the broad spatial distribution of the dunite bands (Figure 10), their variable dip angles (Figure 9), and the lack of early solid-state localization structures in the harzburgites suggests a wide homogeneous distribution of deformation at the scale of the working area at Wadi al Wasit. Once crystallized, the solid-state flow stress of dunite is very similar to that of the host harzburgite owing to the volumetric dominance of olivine allowing continuation of homogenous deformation. This is in strong contrast to the subsequent spatially focused and vertical injection of the websterite dikes (Figures 5, 9, and 10). Here fast fracturing, injection, and rapid crystallization of the websterites generate rigid inclusions in the mechanically soft harzburgites promoting stress concentrations and therefore sites for the onset of solid-state mylonitic deformation as well as later melt percolation forming gabbronorites. Obviously, the presence of melt and the generation of permeability during ongoing deformation results in a runaway process with strain localization and melt focusing, particularly in domains characterized by filter pressing. Note that in the case of shallowly dipping low-angle scenarios, melts have to travel over longer distances along the shear plane to experience similar degrees of cooling compared to a vertical migration scenario. Hence, the melt lubrication efficiency and extraction is enhanced eventually leading to longer-lasting melt weakening in the case of low-angle extensional faults.

Another difference to classical low-angle settings is the limitation of strike-slip shear zones to act as a barrier for both melt migration [*Kaczmarek and Müntener*, 2008] and the infiltration of fluids at temperatures around 800–700°C, the latter often documented by enhanced amounts of hydrous minerals, most notably amphiboles [*Allerton and Macleod*, 1998; *Dijkstra et al*., 2002; *Meshi et al*., 2010]. At these still elevated temperature conditions the vertical orientation of the Wadi al Wasit shear zone prevents a "caprock" function for uprising melts as well as the top-down infiltration of water along steep normal faults in the hanging wall as often observed in the case of midcrustal low-angle normal faults [e.g., *Axen et al*., 2001; *Gottardi et al*., 2011;

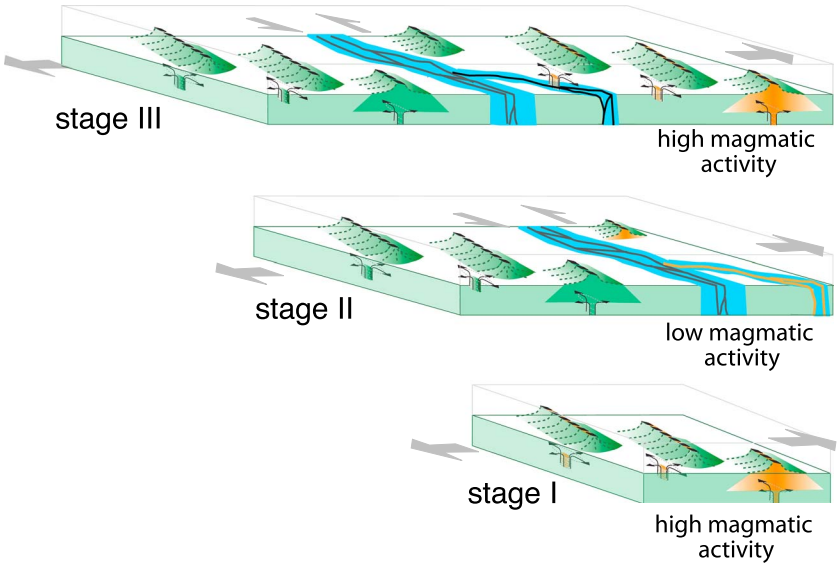

Figure 16. Conceptual model for the evolution ridge segmentation and cooling-induced deformation. Stage I: initial spreading center with different mantle diapirs. Stage II: Spreading leads to cooling and strain accommodation along strike-slip shear zones, which are situated between the mantle diapirs. Shear zone centers act as pathways for ascending melts. Stage III: final stage of spreading. The late magmatic activity in fact may result from a suprasubduction zone scenario [see *Rioux et al*., 2013].

Campani et al., 2012]. Only conditions of limited ductile deformation (<600°C) and ongoing shearing under brittle deformation with associated dilatancy allows for an efficient access of vertically infiltrating seawater as manifest first by the serpentine foliation and later by the cataclastic fault pattern (Figure 5). Similar thermo-hydraulic processes may occur during exhumation of low-angle normal faults into shallower crustal levels. Here, however, intense shearing and fluid infiltration results in a strong serpentinization of the fault core diminishing earlier high-temperature fabrics. In this sense, the Wadi al Wasit strike-slip shear zone provides a unique telescoped view in space and time into the thermomechanical interactions of mantle shear zones ranging form early magmatic to late fluid-assisted deformation stages.

5. Conclusions and Geodynamic Implications

The shear zone of Wadi al Wasit presents an example where early ridge-related injection of melt led to the formation of vertically oriented mechanical anisotropies in form of dikes, which are repeatedly used during progressive spreading and associated solid-state mantle deformation under conditions of retrograde cooling (Figure 12). This evolution is closely linked to the mechanical state of the mantle rocks (Figure 14). In this way, the cyclical brittle fracturing of the mantle rocks accompanied by melt injection at high temperatures (1200–800°C) and the infiltration of water at low temperatures (<500°C) strongly control strain localization in this sequence of the upper mantle (Figures 12 and 14). Despite the important role of both liquid phases, melt and fluids, in strain localization, contrasting rheological effects result for the high- and low-temperature scenarios (Figure 14). In the case of the dikes crystallized at high temperatures, the higher effective viscosity of pyroxene (dominant phase in websterites) compared to the olivine-dominated harzburgite induces stress concentrations, along which ductile deformation is focused (Figure 14). This controls the following: (i) cycles of dike injection and localized ductile shearing, (ii) the energy-controlled shear zone narrowing during retrograde cooling, and (iii) the final embrittlement in the shear zone center (Figures 11, 12, and 14). In the latter case, the facilitated influx of seawater under low-temperature deformation conditions produces reaction-induced weakening and deformation under frictional viscous flow (Figures 11 and 14).

In terms of the vertical orientation combined with the interplay of solid-state deformation and magmatic activity [*Gregg et al*., 2009; *Gerya*, 2012; *Püthe and Gerya*, 2014], the Wadi al Wasit might serve as a mechanical analog for the activity of transform faults close to mid-ocean ridges. Despite the ridge-orthogonal

orientation of the transform faults, cooling associated with progressive spreading probably will lead to similar deformation stages as found in Wadi al Wasit although the geochemical signatures of the melts might differ.

A major open geodynamic question concerns the mechanical and kinematic role of the large-scale strike-slip shear zones so often found in the Semail ophiolite (Figure 16, see also *Michibayashi et al.* [2006]). It is intriguing to see that these strike-slip zones often appear around and in between the inferred mantle diapirs (Figure 16). In addition to earlier studies, which interpreted the shear zones to be obduction related, we clearly favor the interpretation that the initiation of such shear zones reflects domains of strain accommodation of the cooling mantle between hot mantle diapirs. This interpretation is supported by (i) repeated magmatic activity and the related cooling sequence of the websterite and gabbronorite dikes during solid-state deformation as well as (ii) the extremely short time interval (few 10^5 years) [*Rioux et al*., 2013; *Warren et al*., 2005] available for the evolution of the first and second magmatic suite, respectively. Moreover, it is generally accepted that spreading centers (e.g., mid-ocean ridges) do not represent spatially continuous zones of magma expulsion but are segmented and may overlap [e.g., *Perram et al*., 1993; *Nicolas et al*., 2000; *Searle and Escartin*, 2004; *Choi et al*., 2008; *Püthe and Gerya*, 2014]. With progressive cooling, heterogeneous contraction eventually combined with a slight component of oblique rifting during the rapid change from the radial upwelling geometry of a mantle diapir toward an alignment with the rift axis by rift parallel flow, results in a complex 3-D deformation and surface pattern, as recently shown in numerical models by *Burov and Gerya* [2014] (compare with Figures 12 and 16). In this context, strain in the upper mantle might be accommodated by subvertical strike-slip shear zones such as those found in Oman (Figure 16). These strike-slip shear zones thus provide new insights into the processes and geometries of ridge-segmentation in the case of fast-spreading systems. The recent interpretations favoring a suprasubduction zone setting for melt generation of the younger magmatic series in Oman [e.g., *Rioux et al*., 2012, 2013] imply that the Wadi al Wasit shear zone system may even serve as telescoped view for the initiation of a suprasubduction zone spreading scenario.

Appendix: Methods

Lineament maps were drawn based on aerial photographs and Aster satellite images and refined by detailed field mapping along the outcrops in Wadi al Wasit (Oman, Figure 1). Distribution, thickness (measured with a laser device), and specific characteristics of different harzburgitic tectonites and dikes were documented along profiles with particular emphasis to the transition between the different tectonite types. Orientations of foliations, lineations, and dikes were measured. Oriented hand specimens were collected, from which polished thin sections were prepared at orientations perpendicular to the foliation and parallel to the lineation (*X-Z* plane).

Two approaches were followed *to estimate finite strain* of solid-state mylonitic deformation in the harzburgites: (i) Outlines of pyroxene grains on photographs of *X-Z* planes were redrawn for the different tectonite types. The aspect ratios of the pyroxenes were calculated using the digital image analysis software image SXM. The shear strains were then calculated for noncoaxial conditions, assuming initial round pyroxene grains. Note that this first approach yields only minimum estimates of shear strain because the olivine matrix surrounding the clasts took up the majority of deformation. Additionally, (ii) two websterite dikes that were sheared into harzburgitic mylonites served as finite strain markers allowing the calculations of finite strains and the correlation of the macroscopic fabrics ranging from porphyroclastic over protomylonitic to mylonitic fabrics (see section 3). By this approach, the local true shear strains can be evaluated.

Electron backscatter diffraction was applied to obtain information on the grain sizes of olivine, enstatite, and diopside; their volume fractions; and the crystallographic preferred orientation (CPO) of olivine. A detailed description of the preparation procedure as well as the database is given in *Linckens et al*. [2011a, 2011b, 2015]. Furthermore, electron microprobe analysis was performed to obtain the chemical composition of the pyroxenes. These data were used to (i) quantitatively evaluate the effect of second phases, i.e., enstatite and diopside, on deformation of olivine as matrix mineral [*Linckens et al*., 2011b, 2015], (ii) determine the active deformation mechanisms, (iii) apply geothermometers in order to obtain deformation temperatures [*Linckens et al*., 2011a], and (iv) link the corresponding microfabrics with experimental flow laws extrapolated toward the natural conditions [*Linckens et al*., 2011b, 2015]. In the present study we build on these previous results.

Qualitative Raman spectra of the serpentinite samples were acquired with a Jobin Yvon LabRAM-HR800 instrument. The signal was excited by a 532.12 nm frequency-doubled Nd-YAG continuous-wave laser focused through an Olympus BX41 confocal microscope, using a 20 mW beam spot of approximately 1 μm diameter. Reference spectra for the various serpentine minerals were acquired on standards identified by X-ray diffraction (for details see *Lambrecht and Diamond* [2014]).

Acknowledgments

We thank the Ministry of Commerce and Industry of Oman for their support and help in organizing our fieldwork in Oman. Financial support from the Swiss National Science Foundation (project grants 200021-113563, 200020-126560), the electron microprobe facilities (200021-103479/1), and the scanning electron microscope (200021-109369) at the Institute of Geological Sciences, University of Bern is greatly acknowledged. We thank the Editor Claudio Faccenna and two anonymous reviewers for their constructive comments that helped to improve the final presentation. Data are available upon request from the first author.

References

Aharonov, E., J. A. Whitehead, P. B. Kelemen, and M. Spiegelman (1995), Channeling instability of upwelling melt in the mantle, *J. Geophys. Res.*, *100*(B10), 20,433–20,450, doi:10.1029/95JB01307.

Aharanov, E., M. Spiegelman, and P. Kelemen (1997), Three-dimensional flow and reaction in proous media: Implications for the Earth's mantle and sedimentary basins, *J. Geophys. Res.*, *102*, 14,821–14,833, doi:10.1029/97JB00996.

Allerton, S., and C. J. Macleod (1998), Fault-controlled magma transport through the mantle lithosphere at slow-spreading ridges, *Geol. Soc. London Spec. Publ.*, *148*, 29–42.

Anonymous (1972), Penrose field conference on ophiolites, *Geotimes*, *17*, 24–25.

Axen, G., J. Selverstone, and T. Wawrzyniec (2001), High-temperature embrittlement of extensional Alpine mylonite zones in the midcrustal ductile-brittle transition, *J. Geophys. Res.*, *106*(B3), 4337–4348, doi:10.1029/2000JB900372.

Behn, M. D., and G. Ito (2008), Magmatic and tectonic extension at mid-ocean ridges: 1. Controls on fault characteristics, *Geochem. Geophys. Geosyst.*, *9*, Q09O12, doi:10.1029/2008GC001970.

Boschi, C., G. L. Früh-Green, A. Delacour, J. A. Karson, and D. S. Kelley (2006), Mass transfer and fluid flow during detachment faulting and development of an oceanic core complex, Atlantic Massif (MAR 30°N), *Geochem. Geophys. Geosyst.*, *7*, Q01004, doi:10.1029/2005GC001074.

Boudier, E., and A. Nicolas (1985), Harzburgite and lherzolite subtypes in ophiolitic and oceanic environments, *Earth Planet. Sci. Lett.*, *75*, 215–222, doi:10.1016/0012-821X(85)90150-5.

Boudier, F., and R. G. Coleman (1981), Cross section through the peridotite in the semail ophiolite, *J. Geophys. Res.*, *86*, 2573–2592, doi:10.1029/JB086iB04p02573.

Boudier, F., J.-L. Bouchez, A. Nicolas, M. Cannat, G. Ceuleneer, M. Misseri, and R. Montigny (1985), Kinematics of oceanic thrusting in the Oman ophiolite. Model of plate convergence, *Earth Planet. Sci. Lett.*, *75*, 215–222.

Boudier, F., G. Ceuleneer, and A. Nicolas (1988), Shear zones, thrust and related magmatism in the Oman ophiolite: Initiation of thrusting on an oceanic ridge, *Tectonophysics*, *151*, 275–296.

Boudier, F., M. Godard, and C. Armbruster (2000), Significance of gabbronorite occurrence in the crustal section of the Semail ophiolite, *Mar. Geophys. Res.*, *21*, 307–326.

Boudier, F., A. Nicolas, and D. Mainprice (2005), Does anisotropy of thermal contraction control hydrothermal circulation at the moho level below fast spreading oceanic ridges, *Int. Geol. Rev.*, *47*, 101–112, doi:10.2747/0020-6814.47.1.101.

Boudier, F., A. Baronnet, and D. Mainprice (2010), Serpentine mineral replacements of natural olivine and their seismic implications: Oceanic lizardite versus subduction-related antigorite, *J. Petrol.*, *51*(1–2), 495–512, doi:10.1093/petrology/egp049.

Bowden, P. B. (1970), A criterion for plastic inhomogeneous deformation, *Philos. Mag.*, *22*, 455–462.

Braun, M. G., and P. B. Kelemen (2002), Dunite distribution in the Oman ophiolite, Implications for melt flux through porous dunite conduits, *Geochem. Geophys. Geosyst.*, *3*(11), 1–21, doi:10.1029/2001GC000289.

Buck, R., L. Lavier, and A. N. B. Poliakov (2005), Modes of faulting at mid-ocean ridges, *Nature*, *434*, 719–723, doi:10.1038/nature03358.

Burov, E., and T. Gerya (2014), Asymmetric three-dimensional topography over mantle plumes, *Nature*, *513*, 85–89, doi:10.1038/nature13703.

Bystricky, M., and S. Mackwell (2001), Creep of dry clinopyroxene aggregates, *J. Geophys. Res.*, *106*(B7), 13,443–13,454, doi:10.1029/2001JB000333.

Campani, M., A. Mulch, O. Kempf, F. Schlunegger, and N. Mancktelow (2012), Miocene paleotopography of the Central Alps, *Earth Planet. Sci. Lett.*, *337–338*, 174–185.

Casey, M. (1980), Mechanics of shear zones in isotropic dilatant materials, *J. Struct. Geol.*, *2*(1–2), 143–147.

Ceuleneer, G., A. Nicolas, and F. Boudier (1988), Mantle flow patterns at an ocean spreading centre: The Oman peridotites record, *Tectonophysics*, *151*, 1–26.

Ceuleneer, G., M. Monnereau, and I. Amri (1996), Thermal structure of a fossil mantle diapir inferred from the distribution of mafic cumulates, *Nature*, *379*, 149–153.

Choi, E., and W. R. Buck (2010), Constraints on shallow mantle viscosity from morphology and deformation of fast-spreading ridges, *Geophys. Res. Lett.*, *37*, L16302, doi:10.1029/2010GL043681.

Choi, E., L. Lavier, and M. Gurnis (2008), Thermomechanics of mid-ocean ridge segementation, *Phys. Earth Planet. In.*, *171*, 374–386, doi:10.1016/j.pepi.2008.08.010.

Connolly, J. A. D., and Y. Y. Podladchikov (1998), Compaction-driven fluid flow in viscoelastic rock, *Geol. Acta*, *11*(2–3), 55–84.

Dijkstra, A. H., M. R. Drury, and R. M. Frijhoff (2002), Microstructures and lattice fabrics in the Hilti mantle section (Oman Ophiolite): Evidence for shear localization and melt weakening in the crust-mantle transition zone?, *J. Geophys. Res.*, *107*(B11), 2270, doi:10.1029/2001JB000458.

Dijkstra, A. H., M. R. Drury, R. L. M. Vissers, J. Newman, and H. L. M. Van Roermund (2004), Shear zones in the upper mantle: Evidence from alpine- and ophiolite-type peridotite massifs, *Geol. Soc. London Spec. Publ.*, *224*, 11–24.

Dimanov, A., and G. Dresen (2005), Rheology of synthetic anorthite-diopside aggregates: Implications for ductile shear zones, *J. Geophys. Res.*, *110*, B07203, doi:10.1029/2004JB003431.

Dziak, R., C. Fox, and A. Schreiner (1995), The June–July1993 seismo-acoustic event at CoAxial segment, Juan de Fuca Ridge: Evidence for a lateral dike injection, *Geophys. Res. Lett.*, *22*, 135–138, doi:10.1029/94GL01857.

Ebert, A., M. Herwegh, and A. Pfiffner (2007), Cooling induced strain localization in carbonate mylonites within a large-scale shear zone (Glarus thrust, Switzerland), *J. Struct. Geol.*, *29*(7), 1164–1184, doi:10.1016/j.jsg.2007.03.007.

Frets, E. C., A. Tommasi, C. J. Garrido, A. Vauchez, D. Mainprice, K. Targuisti, and I. Amri (2014), The Beni Bousera Peridotite (Rif Belt, Morocco): An oblique-slip low-angle shear zone thinning the subcontinental lithospheric mantle, *J. Petrol.*, *55*, 283–313, doi:10.1093/petrology/egt067.

Fyfe, W. S., N. J. Price, and A. B. Thompson (1978), *Fluids in the Earth's Crust*, Elsevier, Amsterdam.

Gerya, T. (2012), Origin and models of oceanic transform faults, *Tectonophysics*, *522–523*, 34–54, doi:10.1016/j.tecto.2011.07.006.
Gillis, K., et al. (2014), Primitive layered gabbros from fast-spreading lower oceanic crust, *Nature*, *505*, 204–207, doi:10.1038/nature12778.
Gnos, E., and A. Nicolas (1996), Structural evolution of the northern end of the Oman Ophiolite and enclosed granulites, *Tectonophysics*, *254*(1–2), 111–137.
Godard, M., J.-M. Dautria, and M. Perrin (2003), Geochemical variability of the Oman ophiolite lavas; relationship with spatial distribution and paleomagnetic directions, *Geochem. Geophys. Geosyst.*, *4*(6), 8609, doi:10.1029/2002GC000452.
Godard, M., D. Bosch, and F. Einaudi (2006), A MORB source for low-Ti magmatism in the Semail ophiolite, *Chem. Geol.*, *234*, 58–78, doi:10.1016/j.chemgeo.2006.04.005.
Goodwin, L. B., and B. Tikoff (2002), Competency contrast, kinematics and the development of foliations and lineations in the crust, *J. Struct. Geol.*, *24*, 1065–1085, doi:10.1016/S0191-8141(01)00092-X.
Gottardi, R., C. Teyssier, A. Mulch, T. W. Vennemann, and M. L. Wells (2011), Preservation of an extreme transient geotherm in the Raft River detachment shear zone, *Geology*, *39*, 759–762, doi:10.1130/G31834.1.
Gregg, P. M., M. D. Behn, J. Lin, and T. L. Grove (2009), Melt generation, crystallization and extraction beneath segmented oceanic transform faults, *J. Geophys. Res.*, *114*, 1–16, B11102, doi:10.1029/2008JB006100.
Hacker, B. R., and E. Gnos (1997), The conundrum of Samail: Explaining the metamorphic history, *Tectonophysics*, *279*(1–4), 215–226.
Hacker, B. R., J. L. Mosenfelder, and E. Gnos (1996), Rapid emplacement of the Oman ophiolite: Thermal and geochronologic constraints, *Tectonics*, *15*(6), 1230–1247, doi:10.1029/96TC01973.
Hammond, J., J. M. Kendall, J. Wookey, G. Stuart, D. Keir, and A. Ayele (2014), Differentiating flow, melt, or fossil seismic anisotropy beneath Ethiopia, *Geochem. Geophys. Geosyst.*, *15*, 1878–1894, doi:10.1002/2013GC005185.
Havlin, C., E. M. Parmentier, and G. Hirth (2013), Dike propagation driven by melt accumulation at the lithosphere–asthenosphere boundary, *Earth Planet. Sci. Lett.*, *376*, 20–28, doi:10.1016/j.epsl.2013.06.010.
Hayman, N. W., and J. A. Karson (2009), Crustal faults exposed in the Pito Deep Rift: Conduits for hydrothermal fluids on the southeast Pacific Rise, *Geochem. Geophys. Geosyst.*, *10*, Q02013, doi:10.1029/2008GC002319.
Herwegh, M., J. Linckens, A. Ebert, A. Berger, and S. H. Brodhag (2011), The role of second phases for controling microstructural evolution in polymineralic rocks, *J. Struct. Geol.*, *33*, 1728–1750, doi:10.1016/j.jsg.2011.08.011.
Hirth, G., and D. L. Kohlstedt (1996), Water in the oceanic upper mantle: Implications for rheology, melt extraction and the evolution of the lithosphere, *Earth Planet. Sci. Lett.*, *144*(1–2), 93–108.
Hirth, G. and D. Kohlstedt (2003), Rheology of the upper mantle and the mantle wedge: A view from the experimentalists, in *Inside the Subduction Factory*, edited by J. Eiler, AGU, Washington, D. C., doi:10.1029/138GM06.
Hobbs, B. E., B. Mühlhaus, and A. Ord (1990), Instability, softening and localization of deformation, *Geol. Soc. Spec. Publ.*, *54*, 143–165.
Holtzman, B. K., and J. M. Kendall (2010), Organized melt, seismic anisotropy, and plate boundary lubrication, *Geochem. Geophys. Geosyst.*, *11*, Q0AB06, doi:10.1029/2010GC003296.
Holtzman, B. K., N. J. Groebner, M. E. Zimmerman, S. B. Ginsberg, and D. L. Kohlstedt (2003a), Stress-driven melt segregation in partially molten rocks, *Geochem. Geophys. Geosyst.*, *4*, 8607, doi:10.1029/2001GC000258.
Holtzman, B. K., D. L. Kohlstedt, M. E. Zimmermann, F. Heidelbach, T. Hiraga, and J. Hustoft (2003b), Melt segregation and strain partitioning: Implications for seismic anisotropy and mantle flow, *Science*, *301*(5637), 1227–1230, doi:10.1126/science.1087132.
Ildefonse, B., S. Billiau, and A. Nicolas (1995), A detailed study of mantle flow away from diapirs in the Oman Ophiolite, in *Mantle and Lower Crust Exposed in Oceanic Ridges and in Ophiolites*, edited by R. L. M. Vissers and A. Nicolas, pp. 163–177, Kluwer Acad., Norwell, Mass.
Ishikawa, T., K. Nagaishi, and S. Umino (2002), Boninitic volcanism in the oman ophiolite: Implications for thermal condition during transition from spreading ridge to arc, *Geology*, *30*, 899–902, doi:10.1130/0091-7613(2002).
Ishikawa, T., S. Fujisawa, K. Nagaishi, and T. Masuda (2005), Trace element characteristics of the fluid liberated from amphibolite-facies slab: Inference from the metamorphic sole beneath the Oman ophiolite and implication for boninite genesis, *Earth Planet. Sci. Lett.*, *240*(2), 355–377, doi:10.1016/j.epsl.2005.09.049.
Ishizuka, O., T. Kenichiro, and M. K. Reagan (2014), Izu-Bonin-Mariana forearc Crust as a modern ophiolite analogue, *Elements*, *10*, 115–120, doi:10.2113/gselements.10.2.115.
Ito, G., and M. D. Behn (2008), Magmatic and tectonic extension at mid-ocean ridges: 2. Origin of axial morphology, *Geochem. Geophys. Geosyst.*, *9*, Q09O12, doi:10.1029/2008GC001970.
Ito, G., and S. J. Martel (2002), Focusing of magma in the upper mantle through dike interaction, *J. Geophys. Res.*, *107*(B10), ECV 6-1–ECV 6-17, doi:10.1029/2001JB000251.
Jaroslow, G. E., G. Hirth, and H. J. B. Dick (1996), Abyssal peridotite mylonites: Implications for grain-size sensitive flow and strain localization in the oceanic lithosphere, *Tectonophysics*, *256*(1–4), 17–37.
Joan, V. C., and H. J. Lo (1969), Phase relations in the system NaAlSi3O8-CaAl2Si2O8-H2O at low temperatures and pressures, *Proc. Geol. Soc. China (Formosa)*, *12*, 21–29.
Jung, H., and S. Karato (2001), Water-induced fabric transitions in olivine, *Science*, *293*(5534), 1460–1463.
Kaczmarek, M.-A., and O. Müntener (2008), Juxtaposition of melt impregnation and high temperature shear zones in the upper mantle; field and petrological constrains from the Lanzo peridotite (Northern Italy), *J. Petrol.*, *49*, 2187–2220, doi:10.1093/petrology/egn065.
Kaczmarek, M.-A., and O. Müntener (2010), The variability of peridotite composition across a mantle shear zone (Lanzo massif, Italy): Interplay of melt migration and deformation, *Contrib. Mineral. Petrol.*, *160*, 663–679, doi:10.1007/s00410-010-0500-8.
Kaczmarek, M.-A., and A. Tommasi (2011), Anatomy of an extensional shear zone in the mantle (Lanzo massif, Italy), *Geochem. Geophys. Geosyst.*, Q0AG06, doi:10.1029/2011GC003627.
Katayama, I., H. Jung, and S. Karato (2004), New type of olivine fabric from deformation experiments at modest water content and low stress, *Geology*, *32*(12), 1045–1048, doi:10.1130/G20805.1.
Kawakatsu, H., P. Kumar, Y. Takei, M. Shinohara, T. Kanazawa, E. Araki, and K. Suyehiro (2009), Seismic evidence for sharp lithosphere-asthenosphere boundaries of oceanic plates, *Science*, *324*, 499–502, doi:10.1126/science.1169499.
Kelemen, P. B., and H. J. B. Dick (1995), Focused melt flow and localized deformation in the upper mantle: Juxtaposition of replacive dunite and ductile shear zones in the Josephine peridotite, SW Oregon, *J. Geophys. Res.*, *100*, 423–438, doi:10.1029/94JB02063.
Kelemen, P. B., N. Shimizu, and V. J. Salters (1995), Extraction of mid-ocean-ridge basalt from the upwelling mantle by focused flow of melt in dunite channels, *Nature*, *375*(6534), 747–753.
Kelemen, P. B., K. Koga, and N. Shimizu (1997a), Geochemistry of gabbro sills in the crust-mantle transition zone of the Oman ophiolite: Implications for the origin of the oceanic lower crust, *Earth Planet. Sci. Lett.*, *146*, 475–488, doi:10.1016/S0012-821X(96)00235-X.

Kelemen, P. B., G. Hirth, N. Shimizu, M. Spiegelmann, and H. J. Dick (1997b), A review of melt migration processes in the adiabatically upwelling mantle beneath oceanic spreading ridges, *Philos. Trans. R. Soc. A Math. Phys. Eng. Sci.*, *355*(1723), 283–318, doi:10.1098/rsta.1997.0010.

Keller, T., D. A. May, and B. J. Kaus (2013), Numerical modelling of magma dynamics coupled to tectonic deformation of lithosphere and crust, *Geophys. J. Int.*, *195*(3), 1406–1442, doi:10.1093/gji/ggt306.

Koga, K. T., Kelemen, P. B. and N. Shimizu (2001), Petrogenesis of the crust-mantle transition zone and the origin of lower crustal wehrlite in the Oman ophiolites, *Geochem. Geophys. Geosyst.*, *2*(9), doi:10.1029/2000GC00013 .

Lambrecht, G., and L. W. Diamond (2014), Morphological ripening of fluid inclusions and coupled zone-refining in quartz crystals revealed by cathodoluminescence imaging: Implications for CL-petrography, fluid inclusion analysis and trace-element geothermometry, *Geochim. Cosmochim. Acta*, *141*, 381–406.

Linckens, J., M. Herwegh, and O. Muntener (2011a), Linking temperature estimates and microstructures in deformed polymineralic mantle rocks, *Geochem. Geophys. Geosyst.*, *12*, Q08004, doi:10.1029/2011GC003536.

Linckens, J., M. Herwegh, I. Mercolli, and O. Muntener (2011b), Evolution of a polymineralic mantle shear zone and the role of second phases on the localization of deformation, *J. Geophys. Res.*, *116*, B06210, doi:10.1029/2010JB008119.

Linckens, J., M. Herwegh, and O. Muntener (2015), Small quantitiy but large effect—How minor phases control strain localization in the upper mantle, *Tectonophysics*, *643*, 26–43, doi:10.1016/j.tecto.2014.12.008.

Lippard, S. J., A. W. Shelton, and I. G. Gass (1986), *The Ophiolite of Northern Oman*, *Blackwell Sci. Publ. Mem. 11*, Oxford.

Mackwell, S. J. (1991), High-temperature rheology of enstatite—Implications for creep in the mantle, *Geophys. Res. Lett.*, *18*(11), 2027–2030, doi:10.1029/91GL02492.

MacLeod, C. J., C. J. Lissenberg, and L. E. Bibby (2013), "Moist MORB" axial magmatism in the Oman ophiolite: The evidence against a mid-ocean ridge origin, *Geology*, *41*(4), 459–462, doi:10.1130/G33904.1.

Mancktelow, N. S., L. Arbaret, and G. Pennacchioni (2002), Experimental observations on the effect of interface slip on rotation and stabilisation of rigid particles in simple shear and a comparison with natural mylonites, *J. Struct. Geol.*, *24*(3), 567–585, doi:10.1016/S0191-8141(01)00084-0.

Mercier, J. C., and A. Nicolas (1975), Textures and fabrics of upper mantle peridotites as illustrated by basalt xenoliths, *J. Petrol.*, *16*, 454–487.

Meshi, A., F. Boudier, A. Nicolas, and I. Milushi (2010), Structure and tectonics of lower crustal and upper mantle rocks in the Jurassic Mirdita ophiolites, Albania, *Int. Geol. Rev.*, *52*(2–3), 117–141, doi:10.1080/00206810902823982.

Michibayashi, K., and D. Mainprice (2004), The role of pre-existing mechanical anisotropy on shear zone development within oceanic mantle lithosphere: An example from the Oman ophiolite, *J. Petrol.*, *45*(2), 405–414, doi:10.1093/petrology/egg099.

Michibayashi, K., L. Gerbert-Gaillard, and A. Nicolas (2000), Shear sense inversion in the Hilit mantle section (Oman Ophiolite) and active mantle uprising, *Mar. Geophys. Res.*, *21*, 259–268.

Michibayashi, K., I. Toshiki, and K. Kanagawa (2006), The effect of dynamic recrystallization on olivine fabric and seismic anisotropy: Insight from a ductile shear zone, Oman ophiplite, *Earth Planet. Sci. Lett.*, *244*, 695–708, doi:10.1016/j.epsl.2006.02.019.

Moore, D. E., D. A. Lockner, R. Summers, M. Shengli, and J. D. Byerlee (1996), Strength of chrysotile-serpentinite gouge under hydrothermal conditions: Can it explain a weak San Andreas fault?, *Geology*, *24*(11), 1041–1044.

Müntener, O., J. Hermann, and V. Trommsdorff (2000), Cooling history and exhumation of lower-crustal granulite and upper mantle (Malenco, Eastern Central Alps), *J. Petrol.*, *41*(2), 175–200.

Newman, J., W. M. Lamb, M. R. Drury, and R. L. M. Vissers (1999), Deformation processes in a peridotite shear zone: Reaction-softening by an H2O-deficient, continuous net transfer reaction, *Tectonophysics*, *303*(1–4), 193–222.

Nicolas, A. (1986), Structure and petrology of peridotites: Clues to their geodynamic environment, *Rev. Geophys.*, *24*, 875–895, doi:10.1029/RG024i004p00875.

Nicolas, A. (1989), *Structures of Ophiolites and Dynamics of Oceanic Lithosphere*, Kluwer Acad., London.

Nicolas, A., and M. Jackson (1982), High temperature dikes in peridotites: Origin by hydraulic fracturing, *J. Petrol.*, *23*, 568–582.

Nicolas, A., F. Boudier, and G. Ceuleneer (1988), Mantle flow patterns and magma chambers at ocean ridges—Evidence from the Oman ophiolite, *Mar. Geophys. Res.*, *9*(4), 293–310.

Nicolas, A., G. Ceuleneer, F. Boudier, and M. Misseri (1989), Structural mapping in the Oman ophiolites: Mantle diapirism along an oceanic ridge, *Tectonophysics*, *151*, 27–56.

Nicolas, A., F. Boudier, and B. Ildefonse (1994a), Evidence from the Oman ophiolite for active mantle upwelling beneath a fast-spreading ridge, *Nature*, *370*(6484), 51–53.

Nicolas, A., F. Boudier, and B. Ildefonse (1994b), Dike patterns in diapirs beneath oceanic ridges: The Oman ophiolite, in *Magmatic Systems*, edited by M.-P. Ryan, pp. 77–95, Academic Press, Orlando.

Nicolas, A., E. Boudier, B. Ildefonse, and E. Ball (2000), Accretion of Oman and United Arab Emirates ophiolite—Discussion of a new structural map, *Mar. Geophys. Res.*, *21*(3–4), 147–179.

Nicolas, A., B. Ildefonse, F. Boudier, X. Lenoir, and W. Ben Ismail (2000), Dike distribution in Oman-United Arab Emirates ophiolite, *Mar. Geophys. Res.*, *21*, 269–287.

Passarelli, L., E. Rivalta, and A. Shuler (2014), Dike intrusions during rifting episodes obey scaling relationships similar to earthquakes, *Sci. Rep.*, *4*, 3886, doi:10.1038/srep03886.

Pearce, J. A., T. Alabaster, A. W. Shelton, and M. P. Searle (1981), The Oman ophiolite as a cretaceous arc-basin complex: Evidence and implications, *Philos. Trans. R. Soc. London, Ser. A*, *300*(1454), 299–317.

Perram, L. J., M. H. Cormier, M.-H. Cornier, and K. C. Macdonald (1993), Magnetic and tectonic studies of the dueling propagating spreading centers at 20°40′S on the East Pacific Rise: Evidence for Crustal Rotations, *J. Geophys. Res.*, *98*, 13,835–13,850, doi:10.1029/92JB02913.

Püthe, C., and T. Gerya (2014), Dependence of mid-ocean ridge morphology on spreading rate in numerical 3-D models, *Gondwana Res.*, *25*, 270–283, doi:10.1016/j.gr.2013.04.005.

Python, M., and G. Ceuleneer (2003), Nature and distribution of dykes and related melt migration structures in mantle section of the Oman ophiolite, *Geochem. Geophys. Geosyst.*, *4*(7), 1–34, doi:10.1029/2002GC000354.

Regenauer-Lieb, K. (1999), Dilatant plasticity applied to Alpine collision: Ductile void growth in the intraplate area beneath the Eifel volcanic field, *Geodynamics*, *27*, 1–21.

Reid, I., and H. R. Jackson (1981), Oceanic spreading rate and crustal thickness, *Mar. Geophys. Res.*, *5*, 165–172.

Reinen, L. A., J. D. Weeks, and T. E. Tullis (1994), The frictional behavior of lizardite and antigorite serpentinites—Experiments, constitutive models, and implications for natural faults, *Pure Appl. Geophys.*, *143*(1–3), 317–358.

Renner, J., K. Viskupic, G. Hirth, and B. Evans (2003), Melt extraction from partially molten peridotites, *Geochem. Geophys. Geosyst.*, *4*, 8606, doi:10.1029/2002GC000369.

Rioux, M., S. Bowring, P. Kelemen, S. Gordon, F. Dudas, and R. Miller (2012), Rapid crustal accretion and magma assimilation in the Oman-U.A.E. ophiolite: High-precision U-Pb zircon geochronology of the gabbroic crust, *J. Geophys. Res.*, *117*, B07201, doi:10.1029/2012JB009273.

Rioux, M., S. Bowring, P. Kelemen, S. Gordon, R. Miller, and F. Dudas (2013), Tectonic development of the Samail ophiolite: High-precision U-Pb zircon geochronology and Sm-Nd isotopic constraints on crustal growth and emplacement, *J. Geophys. Res. Solid Earth*, *118*, 2085–2101, doi:10.1002/jgrb.50139.

Rybacki, E., M. Gottschalk, R. Wirth, and G. Dresen (2006), Influence of water fugacity and activation volume on the flow properties of fine-grained anorthite aggregates, *J. Geophys. Res.*, *111*, B03203, doi:10.1029/2005JB003663.

Rybacki, E., R. Wirth, and G. Dresen (2010), Superplasticity and ductile fracture of synthetic feldspar deformed to large strain, *J. Geophys. Res.*, *115*, B08209, doi:10.1029/2009JB007203.

Schmerr, N. (2012), The Gutenberg discontinuity: Melt at the lithosphere-asthenosphere boundary, *Science*, *335*, 1480–1483, doi:10.1126/science.1215433.

Scott, D. R. (1988), The competition between percolation and circulation in a deformable porous medium, *J. Geophys. Res.*, *93*, 6451–6462, doi:10.1029/JB093iB06p06451.

Searle, M., and J. Cox (1999), Tectonic setting, origin, and obduction of the Oman ophiolite, *Geol. Soc. Am. Bull.*, *111*, 104–122.

Searle, M. P., and J. Cox (2002), Subduction zone metamorphism during formation and emplacement of the Semail ophiolite in the Oman mountains, *Geol. Mag.*, *139*(3), 241–255.

Searle, M. P., and J. Malpas (1980), Structure and metamorphism of rocks beneath the Semail ophiolite of Oman and their significance in ophiolite obduction, *Trans. R. Soc. Edinburgh*, *71*, 247–262.

Searle, M. P., and J. Malpas (1982), Petrochemistry and origin of sub-ophiolitic metamorphic and related rocks in the Oman Mountains, *J. Geol. Soc. London*, *139*, 235–248.

Searle, M. P., S. J. Lippard, J. D. Smewing, and D. C. Rex (1980), Volcanic rocks beneath the semail ophiolite nappe in the northern Oman mountains and their significance in the mesozoic evolution of tethys, *J. Geol. Soc. London*, *137*(5), 589–604.

Searle, R. C. and J. Escartin (2004), The rheology and morphology of oceanic lithosphere and mid-ocean ridges, in *Mid-ocean Ridges: Hydrothermal Interactions Between the Lithosphere and Oceans*, *Geophys. Monogr. Ser.*, vol. 148, edited by R. C. German, J. Lin, and L. M. Parson, pp. 63–93, AGU, Washington, D. C., doi:10.1029/148GM03.

Sengupta, S. (1997), Contrasting fabrics in deformed dikes and host rocks: Natural examples and a simplified model, in *Evolution of Geological Structures in Micro- to Macro-Scales*, edited by S. Sengupta, pp. 341–372, Chapman and Hall, London.

Skemer, P., J. M. Warren, L. N. Hansen, G. Hirth, and P. B. Kelemen (2013), The influence of water and LPO on initiation and evolution of mantle shear zones, *Earth Planet. Sci. Lett.*, *375*, 222–233.

Spiegelman, M., P. B. Kelemen, and E. Aharonov (2001), Causes and consequences of flow organization during melt transport: The reaction infiltration instability in compactible media, *J. Geophys. Res.*, *106*(B2), 2061–2077, doi:10.1029/2000JB900240.

Takei, Y., and B. K. Holtzman (2009), Viscous constitutive relations of solid-liquid composites in terms of grain boundary contiguity: 3. Causes and consequences of viscous anisotropy, *J. Geophys. Res.*, *114*, B06207, doi:10.1029/2008JB005852.

Tommasi, A., and A. Vauchez (2015), Heterogeneity and anisotropy in the lithospheric mantle, *Tectonophysics*, *661*, 11–37, doi:10.1016/j.tecto.2015.07.026.

Tommasi, A., M. Knoll, A. Vauchez, J. Signorelli, C. Thoraval, and R. Loge (2009), Structural reactivation in plate tectonics controlled by olivine crystal anisotropy, *Nat. Geosci.*, *2*, 422–426, doi:10.1038/ngeo528.

Toy, V. G., J. Newman, W. Lamb, and B. Tikoff (2010), The role of pyroxenites in formation of shear instabilities in the mantle: Evidence from an ultramafic ultramylonite, Twin Sisters massif, Washington, *J. Petrol.*, *51*(1–2), 55–80, doi:10.1093/petrology/egp059.

Ulmer, P., and V. Trommsdorff (1999), Phase relations of hydrous mantle subducting to 300 km. Mantle petrology: Field observations and high pressure experimentation—A tribute to Francis R.(Joe) Boyd, *Geol. Soc. Spec. Publ.*, *6*, 259–281.

Vauchez, A., A. Tommasi, and D. Mainprice (2012), Faults (shear zones) in the Earth's mantle, *Tectonophysics*, *558–559*, 1–27, doi:10.1016/j.tecto.2012.06.006.

Warren, C., R. Parrish, D. J. Waters, and M. P. Searle (2005), Dating the geologic history of Oman's Semail ophiolite: Insights from U-Pb geochronology, *Contrib. Mineral. Petrol.*, *150*, 403–422.

Warren, J. M., and G. Hirth (2006), Grain size sensitive deformation mechanisms in naturally deformed peridotites, *Earth Planet. Sci. Lett.*, *248*, 438–450, doi:10.1016/j.epsl.2006.06.006.

Weatherley, S. M., and R. F. Katz (2012), Melting and channelized magmatic flow in chemically heterogeneous, upwelling mantle, *Geochem. Geophys. Geosyst.*, *13*, Q0AC18, doi:10.1029/2011GC003989.

Weinberg, F. R., and K. Regenauer-Lieb (2010), Ductile fractures and magma migration from source, *Geology*, *38*(4), 363–366, doi:10.1130/G30482.1.

Whattam, S. A., and R. J. Stern (2011), The 'subduction initiation rule': A key for linking ophiolites, intra-oceanic forearcs, and subduction initiation, *Contrib. Mineral. Petrol.*, *162*, 1031–1045, doi:10.1007/s00410-011-0638-z.

Wilson, C. J. L., L. Evans, and C. Delle Piane (2009), Modelling of porphyroclasts in simple shear and the role of stress variations at grain boundaries, *J. Struct. Geol.*, *31*(11), 1350–1364, doi:10.1016/j.jsg.2009.08.001.

Wirsching, U. (1981), Experiments on the hydrothermal formation of calcium zeolites, *Clays Clay Miner.*, *29*, 171–183.

Zimmerman, M. E., and D. L. Kohlstedt (2004), Rheological properties of partially molten lherzolite, *J. Petrol.*, *45*, 275–298.